

Synthesis and Photophysical Properties of Light-Harvesting Arrays Comprised of a Porphyrin Bearing Multiple Perylene-Monoimide Accessory Pigments

Kin-ya Tomizaki,[†] Robert S. Loewe,[†] Christine Kirmaier,[‡] Jennifer K. Schwartz,[‡] Jennifer L. Retsek,[‡] David F. Bocian,^{*,§} Dewey Holten,^{*,‡} and Jonathan S. Lindsey^{*,†}

Department of Chemistry, North Carolina State University, Raleigh, North Carolina 27695-8204, Department of Chemistry, Washington University, St. Louis, Missouri 63130-4899, and Department of Chemistry, University of California, Riverside, California 92521-0403

jlindsey@ncsu.edu

Received April 8, 2002

We present the synthesis and characterization of new light-harvesting arrays containing two, four, or eight perylene-monoimide accessory pigments attached to a zinc porphyrin. Each perylene is substituted with one or three 4-*tert*-butylphenoxy substituents. A 4,3'- or 4,2'-diarylethyne linker joins the perylene *N*-imide position and the porphyrin meso-position, affording divergent or convergent architectures, respectively. The architectures are designed to provide high solubility in organic media and facile perylene-to-porphyrin energy transfer, while avoiding charge-transfer quenching of the excited porphyrin product. For the array containing four perylenes per porphyrin in both nonpolar (toluene) and polar (benzonitrile) media and for the array containing eight perylenes per porphyrin in toluene, the photoexcited perylene-monoimide dye (PMI*) decays rapidly (~3.5 ps) and predominantly ($\geq 90\%$) by energy transfer to the zinc porphyrin to form the excited zinc porphyrin (Zn*), which has excited-state characteristics (lifetime, fluorescence yield) comparable (within ~10%) to those of the isolated chromophore. For the array containing eight perylenes in benzonitrile, PMI* decays ~80% by energy transfer (forming Zn*) and ~20% by hole transfer (forming PMI⁻ Zn⁺); Zn* subsequently decays ~20% by electron transfer (also forming PMI⁻ Zn⁺) and ~80% by the normal routes open to the porphyrin monomer (intersystem crossing, internal conversion, fluorescence). In addition to rapid and efficient perylene-to-porphyrin energy transfer, the broad blue-green to yellow absorption of the perylene dyes complements the blue absorption of the porphyrin, resulting in excellent light harvesting across a significant spectral region. Collectively, the work described herein identifies multiperylene-porphyrin arrays that exhibit suitable photochemical properties for use as motifs in larger light-harvesting systems.

Introduction

Photosynthetic systems deploy large numbers of pigments in antenna complexes to harvest light and funnel the resulting excited-state energy to the reaction centers. Major challenges concerning the design of synthetic light-harvesting arrays entail the choice of light-absorbing components and the appropriate three-dimensional arrangement of the pigments. The resulting array of pigments must absorb strongly across the spectrum of incident light and enable excited-state energy migration among the pigments without competing electron-transfer reactions. A large number of synthetic light-harvesting arrays based on porphyrins have been prepared,¹ wherein the porphyrin serves as a synthetically malleable surrogate for chlorophyll.

Porphyrins absorb intensely in the blue region but only weakly across the remainder of the visible spectrum. One

approach to increase the efficiency of porphyrin-based light-harvesting arrays is to introduce accessory pigments that absorb in regions of the spectrum where porphyrins are relatively transparent. A number of accessory pigments have been examined in conjunction with porphyrins, including carotenoids,² cyanine dyes,³ xanthene dyes,⁴ boron-dipyrrin dyes,⁵ coumarins,⁶ and perylene dyes.^{7–13} Perylenes display many attractive photophysical and chemical features that make them good candidates

(2) Gust, D.; Moore, T. A.; Moore, A. L. *Acc. Chem. Res.* **2001**, *34*, 40–48.

(3) Lindsey, J. S.; Brown, P. A.; Siesel, D. A. *Tetrahedron* **1989**, *45*, 4845–4866.

(4) Lindsey, J. S.; Prathapan, S.; Johnson, T. E.; Wagner, R. W. *Tetrahedron* **1994**, *50*, 8941–8968.

(5) Li, F.; Yang, S. I.; Ciringh, Y.; Seth, J.; Martin, C. H., III; Singh, D. L.; Kim, D.; Birge, R. R.; Bocian, D. F.; Holten, D.; Lindsey, J. S. *J. Am. Chem. Soc.* **1998**, *120*, 10001–10017.

(6) Hecht, S.; Vladimirov, N.; Fréchet, J. M. J. *J. Am. Chem. Soc.* **2001**, *123*, 18–25.

(7) Miller, M. A.; Lammi, R. K.; Prathapan, S.; Holten, D.; Lindsey, J. S. *J. Org. Chem.* **2000**, *65*, 6634–6649.

(8) Prathapan, S.; Yang, S. I.; Seth, J.; Miller, M. A.; Bocian, D. F.; Holten, D.; Lindsey, J. S. *J. Phys. Chem. B* **2001**, *105*, 8237–8248.

(9) Yang, S. I.; Prathapan, S.; Miller, M. A.; Seth, J.; Bocian, D. F.; Lindsey, J. S.; Holten, D. *J. Phys. Chem. B* **2001**, *105*, 8249–8258.

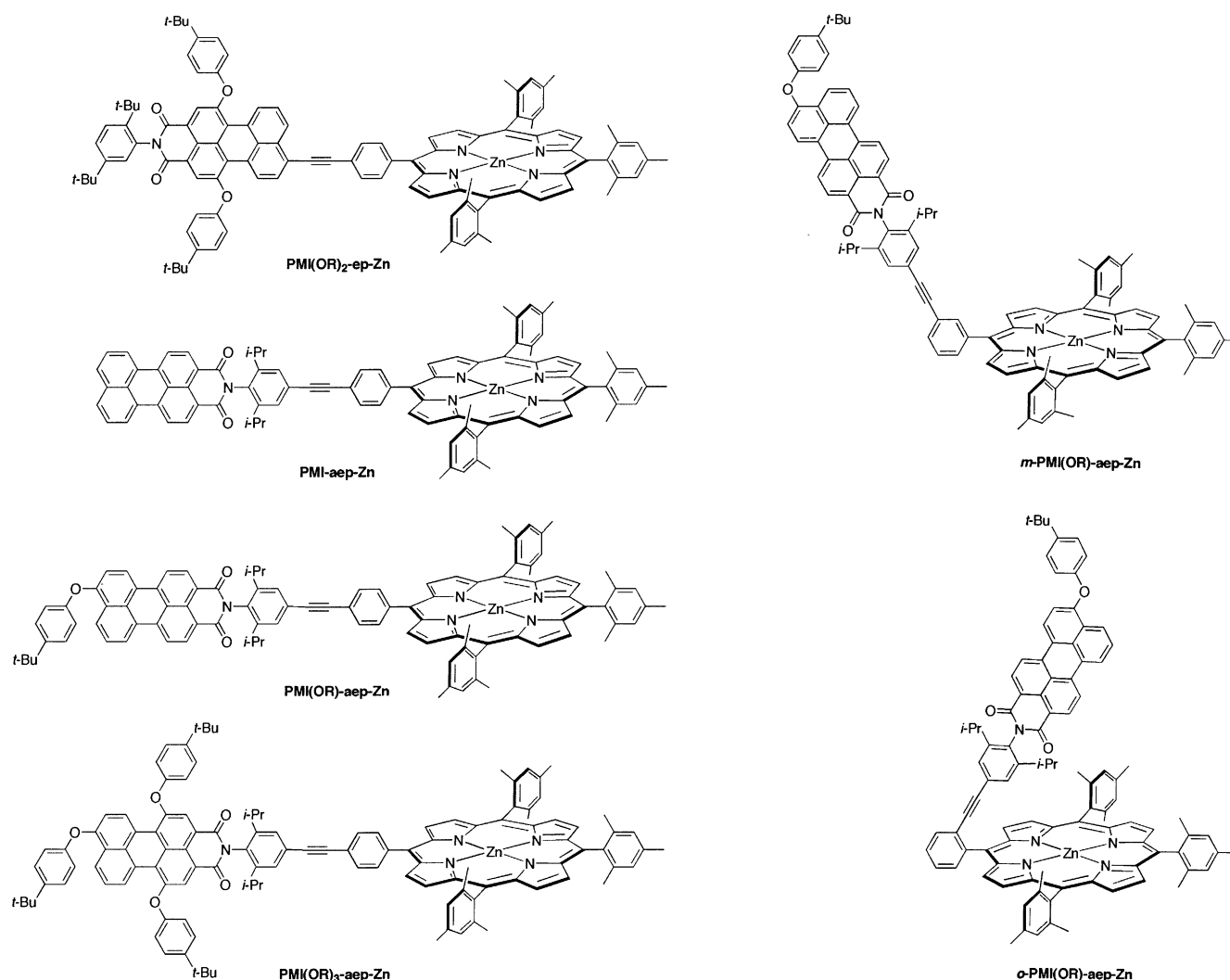
[†] North Carolina State University. Fax: 919-513-2830.

[‡] Washington University.

[§] University of California at Riverside.

(1) Burrell, A. K.; Officer, D. L.; Plieger, P. G.; Reid, D. C. W. *Chem. Rev.* **2001**, *101*, 2751–2796.

CHART 1



for accessory pigments with porphyrins. From a photo-physical standpoint, perylenes have moderately large extinction coefficients in the region between the porphyrin Soret and Q bands (450–500 nm),¹⁴ very high fluorescence quantum yields,^{14,15} and long singlet excited-state lifetimes.¹⁶ From a chemical standpoint, perylenes are amenable to a modular building block synthesis, have good solubility in organic solvents, and are uncharged, thereby facilitating chromatographic purification.

In our prior studies of perylene–porphyrin dyads, we found that both perylene-bis(imide) dyes and perylene-monoimide dyes undergo rapid excited-state energy

transfer to an adjoining porphyrin but that the perylene-bis(imide) dyes are much more prone to competitive excited-state electron-transfer reactions.^{8–11} Accordingly, for light-harvesting applications, we have focused on the use of perylene-monoimide dyes as accessory pigments with porphyrins. A major objective is to design soluble perylene–porphyrin building blocks that provide good spectral coverage, undergo energy transfer without competing electron-transfer reactions in nonpolar or polar media, and can be elaborated into oligomeric structures. To begin identifying suitable perylene–porphyrin motifs, we initially prepared and characterized dyads having a common zinc porphyrin and differing only in the nature of the substituted perylene, linker, and site of attachment (*o*-, *m*-, *p*-) on the *meso*-aryl ring of the porphyrin (Chart 1).¹² Suitable solubility and photochemical properties were obtained with perylenes that (1) bear one or three 4-*tert*-butylphenoxy substituents and (2) are linked to the porphyrin via a diarylethyne linker that bridges the perylene *N*-imide position and the porphyrin *meso*-position.

In this paper, we present the synthesis and selected physical properties of several perylene–porphyrin light-harvesting arrays using the types of perylenes and linkers found to be viable in the dyad studies. The

(10) Yang, S. I.; Lammi, R. K.; Prathapan, S.; Miller, M. A.; Seth, J.; Diers, J. A.; Bocian, D. F.; Lindsey, J. S.; Holten, D. *J. Mater. Chem.* **2001**, *11*, 2420–2430.

(11) Kirmaier, C.; Yang, S. I.; Prathapan, S.; Miller, M. A.; Diers, J. A.; Bocian, D. F.; Lindsey, J. S.; Holten, D. *Res. Chem. Intermed.*, in press.

(12) Loewe, R. S.; Tomizaki, K.-Y.; Thamyongkit, P.; Chevalier, F.; Kirmaier, C.; Schwartz, J. K.; Diers, J. R.; Bocian, D. F.; Holten, D.; Lindsey, J. S. Manuscripts in preparation.

(13) Hayes, R. T.; Wasielewski, M. R.; Gosztoła, D. *J. Am. Chem. Soc.* **2000**, *122*, 5563–5567.

(14) Langhals, H. *Chem. Ber.* **1985**, *118*, 4641–4645.

(15) (a) Rademacher, A.; Märkle, S.; Langhals, H. *Chem. Ber.* **1982**, *115*, 2927–2934. (b) Ebeid, E. M.; El-Daly, S. A.; Langhals, H. *J. Phys. Chem.* **1988**, *92*, 4565–4568.

(16) Ford, W. E.; Kamat, P. V. *J. Phys. Chem.* **1987**, *91*, 6373–6380.

systems described contain multiple (2, 4, or 8) perylene-monoimide accessory pigments joined to a zinc porphyrin. In each array, the perylenes are attached to the 2,6- or 3,5-positions of the *meso*-phenyl ring of the porphyrin via an arylolethynylphenyl (aep) linker. The resulting projection of the perylene out of the plane of the porphyrin should suppress cofacial aggregation of the porphyrins in solution, thereby affording highly soluble light-harvesting arrays. Isopropyl groups on the 2,6-positions of the aryl unit attached to the *N*-imide site cause the perylene and the *N*-aryl unit to be essentially perpendicular, thereby enhancing the solubility of the perylene dye. The photochemical properties of the arrays have been surveyed by static absorption and fluorescence measurements to identify multiperylene–porphyrin constructs suitable for further study. Fluorescence lifetime and time-resolved absorption measurements were performed on the largest architectures, which contain four or eight perylenes per porphyrin. This work is a prelude to the development of multiperylene–porphyrin building blocks for elaboration into oligomeric light-harvesting arrays.

Results and Discussion

(1) Synthetic Strategies. The preparation of the perylene–porphyrin arrays follows one of two general approaches. In approach A, a bis(perylenaldehyde) is prepared by the Sonogashira coupling of a bromo- or ethynylperylene with a diethynyl- or dibromobenzaldehyde. The resulting bis(perylenaldehyde) can then be used as a starting material in a mixed-aldehyde condensation (forming an A_3B -porphyrin), can be reacted with a dipyrromethane (forming a *trans*- A_2B_2 -porphyrin), or can be reacted with pyrrole (forming an A_4 -porphyrin). In approach B, a mixed-aldehyde condensation affords a diethynyl A_3B -porphyrin, which upon Sonogashira coupling with a suitable bromoperylene affords the perylene–porphyrin light-harvesting array. The two approaches differ only in the order of the Sonogashira and porphyrin-forming reactions. We note that the mixed-aldehyde route to A_3B -porphyrins is somewhat unattractive, typically producing a mixture of six porphyrins that is separated by chromatography. However, the existing rational approaches for the preparation of A_3B -porphyrins have not proved compatible with three mesityl groups,¹⁷ as are used in the perylene–porphyrin arrays described herein. The mixed-aldehyde condensations¹⁸ with mesitaldehyde were performed using $BF_3 \cdot O(Et)_2$ –ethanol cocatalysis¹⁹ at a higher concentration²⁰ (~70 mM concentrations of pyrrole and total ArCHO) than typically employed (10 mM).

(2) Convergent Perylene–Porphyrin Array. The positioning of a perylene-monoimide at the 2,6-positions of the *meso*-aryl ring of the tetraarylporphyrin was quite attractive as a means of covering the face of the porphyrin, thereby suppressing porphyrin–porphyrin aggrega-

tion.²¹ We decided to employ approach B in the synthesis of this target perylene–porphyrin array. The Sonogashira coupling of commercially available 2,6-dichlorobenzaldehyde and (trimethylsilyl)acetylene was performed under the conditions developed by Buchwald and Fu,²² which allow for the Sonogashira coupling of aryl bromides at room temperature (Scheme 1). We employed the catalytic system of $Pd(PhCN)_2Cl_2$, CuI, and $P(t-Bu)_3$ in dioxane containing diisopropylamine. The reaction was performed at 70 °C with excess (trimethylsilyl)acetylene (1.75 equiv per chloride) to overcome the low reactivity of the aryl chlorides. Analysis of the crude reaction mixture by GC after 24 h revealed no starting material or monocoupled product. Purification by filtration through silica, Kugelrohr distillation, and column chromatography afforded **1** in 37% yield.

Aldehyde **1**, mesitaldehyde, and pyrrole (71 mM) were then subjected to a mixed-aldehyde condensation with $BF_3 \cdot O(Et)_2$ –ethanol cocatalysis¹⁹ in $CHCl_3$ at room temperature for 1.5 h, followed by oxidation with DDQ. The resulting mixture of porphyrins was treated to the standard conditions for zinc metalation (5 equiv of $Zn(OAc)_2 \cdot 2H_2O$ in $CHCl_3/MeOH$ at room temperature).⁴ However, these conditions failed to furnish the zinc chelate. Therefore, the metalation reaction was performed at 100 °C using DMF as solvent. Purification by column chromatography furnished *meso*-tetramesitylporphyrin zinc(II) as the dominant porphyrin product and the desired porphyrin **2** in only 1.1% yield. The very low yield with 2,6-diethynylbenzaldehyde is in accord with the low yields obtained with other aldehydes bearing large groups at the 2,6-positions such as 2,6-bis(trifluoromethyl)benzaldehyde,¹⁹ 2,4,6-triphenylbenzaldehyde,²³ 2,6-dibromobenzaldehyde,²⁴ or 9-anthraldehyde.²⁵ Treatment of **2** with TBAF in $CHCl_3/THF$ (1:1) afforded the 2,6-diethynyl-substituted zinc porphyrin **2'** in 82% yield.

The last step in the preparation of the 2,6-disubstituted perylene–porphyrin array **4** employed Sonogashira coupling of **2'** and **2** equiv of bromoperylene building block **3**.¹² The conditions for this coupling reaction were identical to those developed for the Sonogashira coupling of iodoporphyrins and ethynylporphyrins²⁶ with the following modifications: (1) the reaction temperature was 60 °C to facilitate coupling of the less reactive bromo substituent;²⁷ (2) a 10:1 ratio of toluene/TEA was employed; (3) the reaction was performed at 10 mM perylene; and (4) the ratio of [bromoperylene]:[$Pd_2(dba)_3$]:[$P(o-tol)_3$] = 1:0.1:0.6.¹² Purification using a three-column proce-

(21) In preliminary work, a *trans*- A_2B_2 porphyrin bearing two perylenes was prepared (wherein an *o*-ethynylphenyl (ep) unit bridges the 9-position of the perylene-monoimide and the *meso*-position of the porphyrin). Two atropisomers were obtained. However, each atropisomer proved unsuited for photochemical applications because of the strong electronic coupling afforded by the ethynylphenyl linker (see the Supporting Information).

(22) Hundertmark, T.; Littke, A. F.; Buchwald, S. L.; Fu, G. C. *Org. Lett.* **2000**, *12*, 1729–1731.

(23) (a) Suslick, K. S.; Fox, M. M. *J. Am. Chem. Soc.* **1983**, *105*, 3507–3510. (b) Sugimoto, H.; Aida, T.; Inoue, S. *Macromolecules* **1990**, *23*, 2869–2875.

(24) Collman, J. P.; Hampton, P. D.; Brauman, J. I. *J. Am. Chem. Soc.* **1990**, *112*, 2986–2998.

(25) Cense, J.-M.; Le Quan, R.-M. *Tetrahedron Lett.* **1979**, 3725–3728.

(26) Wagner, R. W.; Ciringh, Y.; Clausen, C.; Lindsey, J. S. *Chem. Mater.* **1999**, *11*, 2974–2983.

(27) Loewe, R. S.; Lammi, R. K.; Diers, J. R.; Kirmaier, C.; Bocian, D. F.; Holtz, D.; Lindsey, J. S. *J. Mater. Chem.* **2002**, *12*, 1530–1552.

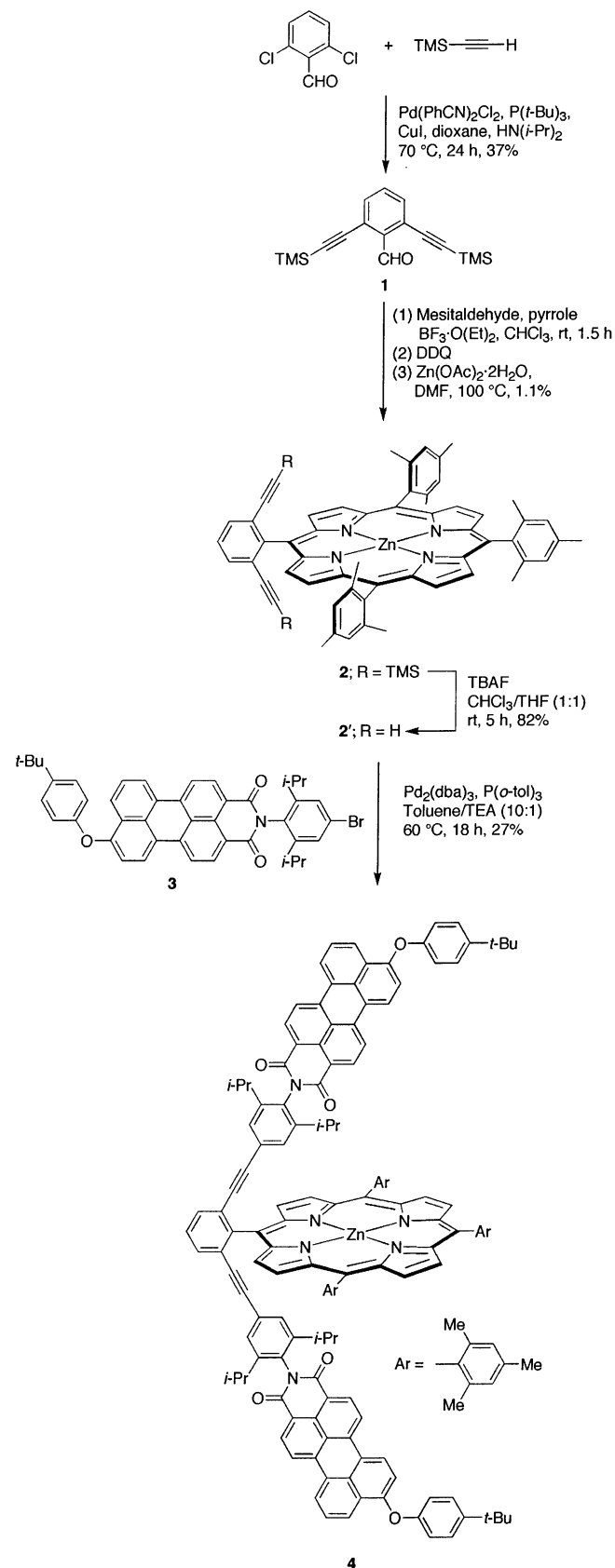
(17) Rao, P. D.; Dhanalekshmi, S.; Littler, B. J.; Lindsey, J. S. *J. Org. Chem.* **2000**, *65*, 7323–7344.

(18) Lindsey, J. S.; Prathapan, S.; Johnson, T. E.; Wagner, R. W. *Tetrahedron* **1994**, *50*, 8941–8968.

(19) Lindsey, J. S.; Wagner, R. W. *J. Org. Chem.* **1989**, *54*, 828–836.

(20) Wagner, R. W.; Li, F.; Du, H.; Lindsey, J. S. *Org. Process Res. Dev.* **1999**, *3*, 28–37.

SCHEME 1



26 afforded **4** in 27% yield. Proton NMR analysis confirmed that the perylenes project over the face of the porphyrin macrocycle, as evidenced by the upfield reso-

nances of the two isopropyl groups and the hydrogens on the aryl group attached to the *N*-imide position of the perylene. This architecture is designed to suppress cofacial aggregation of porphyrins in solution.

(3) Divergent Perylene–Porphyrin Arrays. The attachment at the 3,5-positions of the porphyrin *meso*-aryl ring causes each perylene-monoimide to project away from and out of the plane of the porphyrin.

Arrays Incorporating Mono-Aryloxyperylene. The reaction of aldehyde **5**,⁵ mesitaldehyde, and pyrrole (72 mM) with $\text{BF}_3\cdot\text{O}(\text{Et})_2$ –ethanol cocatalysis¹⁹ in CHCl_3 at room temperature followed by oxidation with DDQ afforded a mixture of porphyrins (Scheme 2). Treatment of the partially purified porphyrin mixture with $\text{Zn}(\text{OAc})_2\cdot 2\text{H}_2\text{O}$ followed by column chromatography afforded the zinc porphyrin building block **6** in 14% yield. The reaction of porphyrin **6** with 2 equiv of bromoperylene **3** under Pd-coupling conditions afforded bis(peryleneporphyrin) **7** in 13% yield.

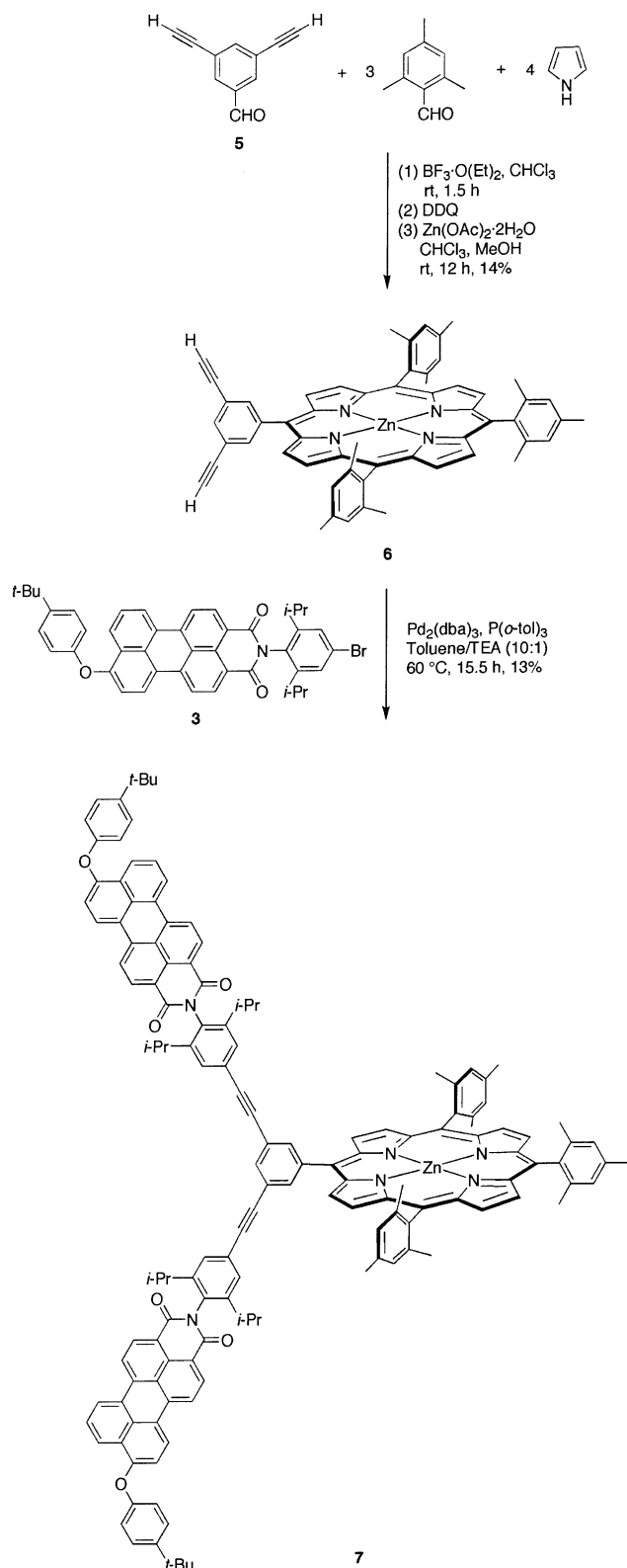
We attempted to prepare a *trans*- A_2B_2 -porphyrin array bearing four perylene accessory pigments using approach B. Aldehyde **5** and 5-mesityldipyrromethane (**8**)²⁸ were condensed using TFA in CH_2Cl_2 at room temperature for 30 min, followed by oxidation with DDQ (Scheme 3). These conditions are known to proceed without detectable formation of byproducts derived from acidolysis of 5-mesityldipyrromethane, followed by undesired recombination (i.e., scrambling).²⁹ Metalation with $\text{Zn}(\text{OAc})_2\cdot 2\text{H}_2\text{O}$ afforded zinc porphyrin **9** in 15% yield. The tetraethynylporphyrin **9** serves as a benchmark compound for spectroscopic characterization. Attempts to react **9** with bromoperylene **3** under Pd-coupling conditions resulted in a crude mixture containing the expected tetrakis(peryleneporphyrin) array, but insufficient solubility in toluene and THF precluded purification.

Arrays Incorporating Tris(aryloxy)perylene. The higher solubility of perylenes bearing three aryloxy groups (1-, 6-, and 9-positions) versus only one aryloxy group (9-position) prompted us to employ the tris(aryloxy)perylene **10**¹² and **11**¹² as precursors to perylene–porphyrin arrays. We explored two routes for the Sonogashira coupling leading to a suitable perylene–aldehyde (**13**) for use in approach A (Scheme 4). The first route employs bromoperylene **10** and 3,5-diethynylbenzaldehyde (**5**) (2:1 ratio) as the starting materials. The reaction under copper-free conditions, similar to those employed for the Sonogashira coupling of two porphyrins²⁶ but with the ratios employed for **4**, afforded only a small amount (8.9%) of perylene–aldehyde **13** (entry 1, Table 1). The same reaction in the presence of CuI failed to produce perylene–aldehyde **13** (entry 2). We next examined the reaction with the reverse ethyne–bromo substitution pattern on the perylene and benzaldehyde. The reaction of ethynylperylene **11** and 3,5-dibromobenzaldehyde (**12**) (2:1 ratio) with CuI cocatalysis afforded **13** in 31% yield (entry 3). A further increase in the amount of perylene **11** (2.4:1 ratio) gave **13** in 66% yield (entry 4). Repetition of this reaction furnished **13** in 83% yield. While of limited scope, the survey of the Sonogashira

(28) Littler, B. J.; Miller, M. A.; Hung, C.-H.; Wagner, R. W.; O'Shea, D. F.; Boyle, P. D.; Lindsey, J. S. *J. Org. Chem.* **1999**, *64*, 1391–1396.

(29) Littler, B. J.; Ciringh, Y.; Lindsey, J. S. *J. Org. Chem.* **1999**, *64*, 2864–2872.

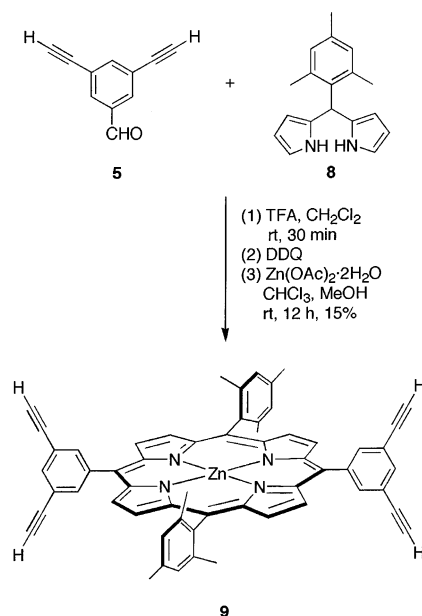
SCHEME 2



reaction of perylene **10** or **11** with aldehyde **5** or **12** revealed important reactivity differences between a bromoperylene and an ethynylperylene. Compound **13** proved to be very soluble, thereby enabling porphyrin-forming reactions.

An A_3B -porphyrin was prepared using a mixed-aldehyde condensation of perylene–aldehyde **13**, mesitalde-

SCHEME 3



hyde, and pyrrole (71 mM) with $\text{BF}_3 \cdot \text{O}(\text{Et})_2$ –ethanol cocatalysis¹⁹ in CHCl_3 (Scheme 4). Oxidation with DDQ followed by zinc metalation afforded perylene–porphyrin **14** in 18% yield, following preparative-scale size exclusion chromatography (SEC) and one silica gel column. This array contains two perylenes attached at the 3,5-positions of the porphyrin *meso*-aryl ring.

The condensation of perylene–aldehyde **13** with 5-mesityldipyrrromethane (**8**) was carried out under nonscrambling reaction conditions²⁹ [(1) TFA, CH_2Cl_2 , room temperature, 30 min; (2) DDQ]. Metalation of the free base porphyrin using $\text{Zn}(\text{OAc})_2 \cdot 2\text{H}_2\text{O}$ followed by purification afforded perylene–porphyrin **15** in 28% yield (Scheme 5). This array contains four perylenes attached at the 3,5-positions of the *trans*-porphyrin *meso*-aryl rings. A space-filling model of **15** is shown in Figure 1.

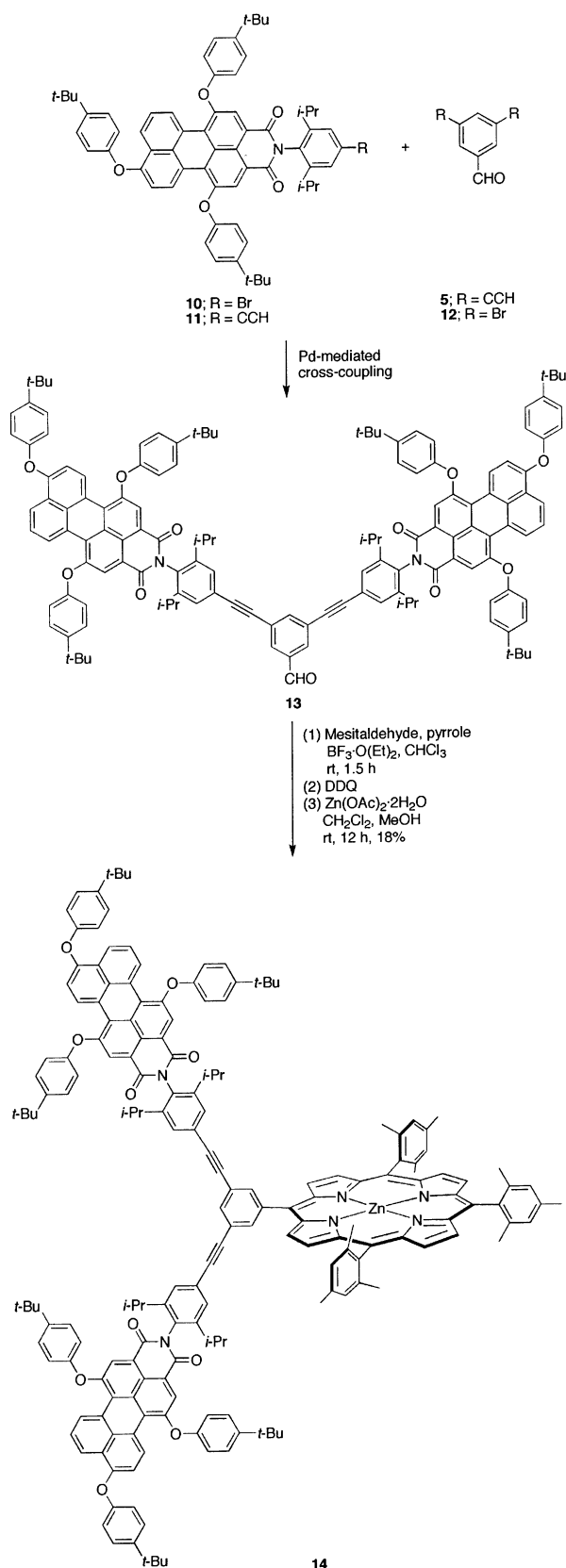
The condensation of perylene–aldehyde **13** and pyrrole was performed in the presence of $\text{BF}_3 \cdot \text{O}(\text{Et})_2$ and NaCl in CH_2Cl_2 at room temperature for 1 h (Scheme 6). The addition of NaCl to the porphyrin-forming reaction has been shown to increase the yield of porphyrin by up to 2-fold in some cases.³⁰ Oxidation with DDQ followed by zinc insertion afforded perylene–porphyrin **16** in 31% yield. This perylene–porphyrin light-harvesting array contains eight perylene accessory pigments, with exhaustive substitution at the 3,5-positions of each of the four *meso*-phenyl rings of the porphyrin. The presence of eight perylenes and 24 aryloxy substituents results in a sizable mass (8264 Da) for the array to which the porphyrin makes a minor contribution.

(4) Chemical Characterization. Each perylene–porphyrin array was characterized by analytical SEC, thin-layer chromatography, laser desorption mass spectrometry (LDMS), ^1H NMR spectroscopy, absorption spectroscopy, and fluorescence emission spectroscopy.

SEC Behavior. Each purified array exhibited a single sharp peak in the analytical SEC chromatogram. The retention times were consistent with molecular sizes: **4**

(30) (a) Li, F.; Yang, K.; Tyhonas, J. S.; MacCrum, K. A.; Lindsey, J. S. *Tetrahedron* **1997**, *53*, 12339–12360. (b) Geier, G. R., III; Riggs, J. A.; Lindsey, J. S. *J. Porphyrins Phthalocyanines* **2001**, *5*, 681–690.

SCHEME 4



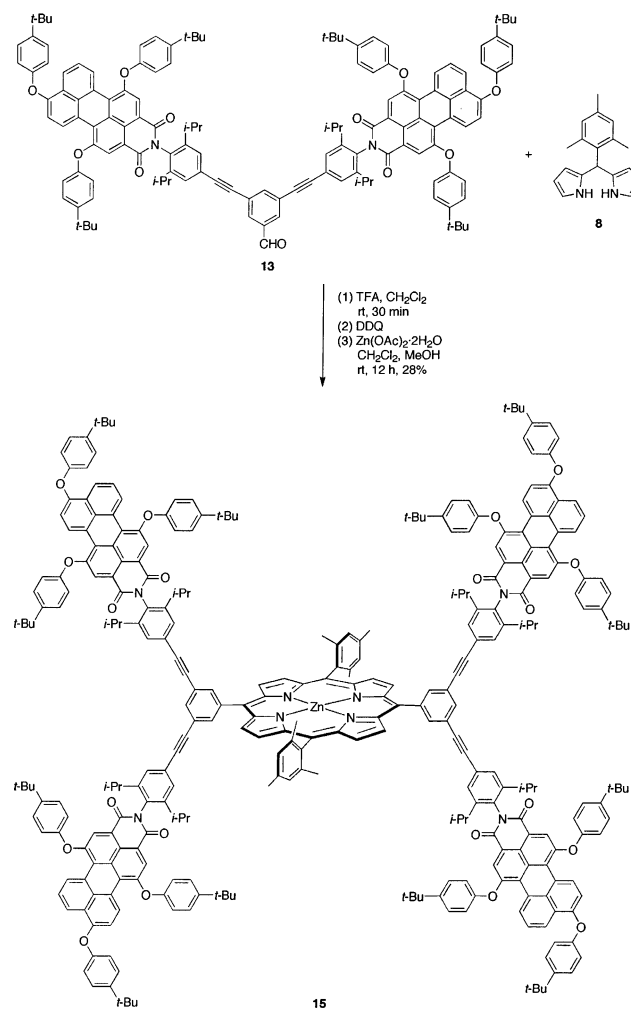
(9.7 min), **7** (9.5 min), **14** (9.2 min), **15** (8.7 min), and **16** (8.4 min). In addition to providing evidence for purity, in a few instances, evidence also was obtained concerning the relative hydrodynamic volumes of isomeric arrays.

TABLE 1. Conditions for Sonogashira Reaction Yielding Bis(perylen)aldehyde 13^a

entry	copper source	ligand	temp (°C)	reactants (mM)	yield (%)
1	none	P(<i>o</i> -tol) ₃	60	10 (10) 5 (5)	8.9
2	CuI	PPh ₃	50	10 (10) 5 (5)	0
3	CuI	PPh ₃	50	11 (10) 12 (5)	31
4	CuI	PPh ₃	50	11 (12) 12 (5)	66, 83

^a Toluene/TEA (5:1) as solvent; Pd₂(dba)₃ as palladium source for all entries.

SCHEME 5



For example, **4** and **7** have identical molecular weight yet showed a difference in retention times of 0.2 min, which stems from the convergent versus divergent architecture of the perylene–porphyrin arrays. A similar observation was noted for the $\alpha\alpha$ - versus $\alpha\beta$ -atropisomers of a perylene–porphyrin joined via a 2-ethynylphenyl linker (see the Supporting Information).

Solubility. High solubility in a variety of solvents is critical for purification, characterization, and photochemical studies. We have found each of the perylene–porphyrin arrays to be sufficiently soluble for routine chemical processing. The highest solubility was noted for arrays **14**–**16**, wherein each perylene bears three 4-*tert*-butylphenoxy substituents. These arrays are soluble in hexanes/CH₂Cl₂ (1:1) for preparative chromatography, are soluble in minimal amounts of CDCl₃ for NMR

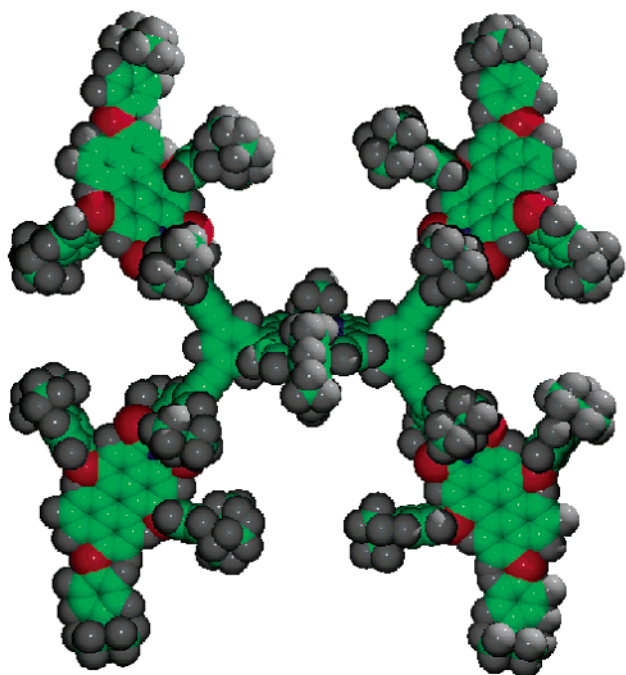


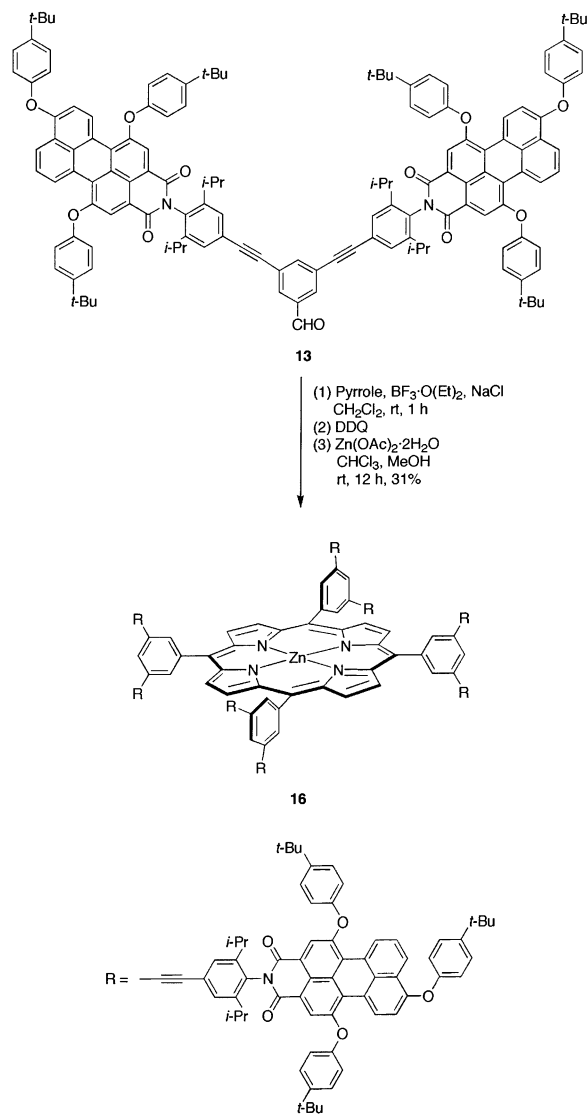
FIGURE 1. Space-filling model of perylene–porphyrin array **15** showing the projection of the perylenes with respect to the porphyrin.

spectroscopy, and afford 10 mM solutions in toluene, CHCl_3 , CH_2Cl_2 , THF, or benzonitrile. The high solubility of these perylene–porphyrin model compounds augurs well for the use of these motifs in larger light-harvesting arrays.

(5) Photophysical Characterization of Benchmark Perylene Dyes. The 4-*tert*-butylphenoxy substituents were introduced as a means of imparting greater solubility to the perylene–porphyrin arrays. The presence of the aryloxy substituents causes significant changes in the absorption spectrum of the perylene dye. Benchmark perylene-monoimide dyes bearing zero, one, or three 4-*tert*-butylphenoxy substituents were prepared and characterized; these dyes are PMI-1,³¹ PMI-2,³² PMI(OR),¹² and **11**,¹² with the latter hereafter termed PMI(OR)₃' for comparison purposes (Chart 2). A summary of the photophysical properties of these three reference compounds is given in Table 2.

The absorption spectra of the benchmark perylene dyes are shown in Figure 2 (solid). The perylene-monoimides display a broad absorption manifold (fwhm ~ 75 nm) consisting of a series of substantially overlapping vibronic transitions with a modest molar extinction coefficient ($\epsilon_{\text{max}} \sim 35\,000\ \text{M}^{-1}\ \text{cm}^{-1}$). The unsubstituted perylene-monoimide exhibits the (0,0) band at 507 nm and the comparably intense (1,0) band at 479 nm with progressively weaker (2,0) and (3,0) features at approximately 455 and 430 nm. The presence of one or three 4-*tert*-butylphenoxy substituents results in a bathochromic shift of approximately 30 nm, such that the origin band moves from 506 nm in PMI-2 to 532 nm in PMI(OR) and 536 nm in PMI(OR)₃' (Table 2). Thus, the dominant contribu-

SCHEME 6



tion to the spectral shift stems from substitution at the 9-position of the perylene; further substitution of two aryloxy groups at the flanking positions (1-, 6-) of the perylene has comparatively little effect on the spectral properties.

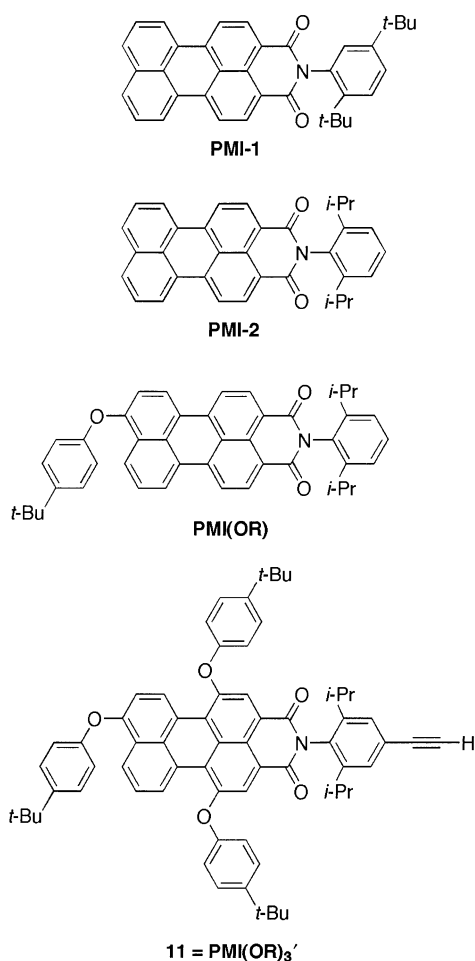
The larger substituent effect at the perylene 9-position derives from the high electron density at this site relative to other sites.³³ In addition to the substantial spectral shifts shown in Figure 2 for the dyes that employ the solubilizing aryloxy groups, we have found that incorporation of ethyne or ethynylphenyl groups at the 9-position causes 12 or 25 nm red shifts, respectively, in the origin transition of perylene-monoimide PMI-1, which differs from PMI-2 only in the substituents on the aryl ring at the *N*-imide position (Chart 2).¹⁰ Even larger shifts have been seen in a perylene-monoimide dye bearing an *N*-pyrrolidinyl substituent at the 9-position (along with 4-*tert*-butylphenoxy substituents at the 1- and 6-positions), which moves the origin band by about 95 nm to 601 nm.³⁴ Such a large shift in this band and the

(31) Feiler, L.; Langhals, H.; Polborn, K. *Liebigs Ann.* **1995**, 1229–1244.

(32) Quante, H.; Müllen, K. *Angew. Chem.* **1995**, 107, 1487–1489.

(33) Adachi, M.; Murata, Y.; Nakamura, S. *J. Phys. Chem.* **1995**, 99, 14240–14246.

CHART 2

TABLE 2. Absorption and Fluorescence Properties of Perylene Benchmark Dyes^a

compound	λ_{abs} (log ϵ)	fwhm (nm)		Φ_f	τ (ns)
		λ_{exc} (nm)	λ_{em} (nm)		
PMI-2	479 (4.5), 506 (4.5) ^b	75	529, 569	0.91 ^c	5.0 ^d
PMI(OR)	507 (4.6), 532 (4.5)	82	567, 611	0.82	4.8
PMI(OR) ₃ '	511 (4.5), 536 (4.6)	71	577, 623	0.86	5.0

^a All data for toluene at room temperature with $\lambda_{\text{exc}} = 490$ nm. Only the wavelengths of the (0,0) and (1,0) absorption bands and the (0,0) and (0,1) emission bands are listed, although (at least) four overlapping vibronic bands are observed in each spectrum. The errors in the fluorescence lifetimes are ± 0.2 ns. ^b Values from literature = 484 (4.5), 506 (4.5).⁴⁷ ^c Value from literature = 0.90.⁴⁸ ^d Value from literature = 4.6 ns.⁴⁸ The value for a related compound (PMI-1) is 4.8 ± 0.1 ns.

corresponding emission features would be too large for our purposes, as this would reduce spectral overlap for a through-space contribution to energy transfer with the porphyrin (which supplements the through-bond contribution¹⁰). Perylene-monoimide dyes each bearing four aryloxy substituents (at the 1-, 6-, 7-, and 12-positions) have also been prepared, but spectral data have not been reported.³⁵

Each of the benchmark perylene-monoimide dyes has a broad fluorescence contour that is approximately a

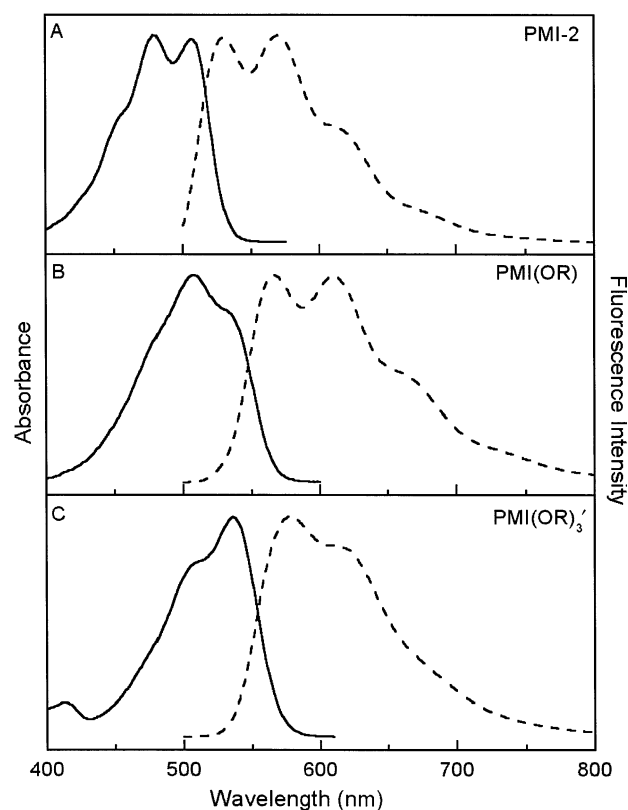


FIGURE 2. Absorption spectra (solid) and fluorescence spectra (dashed) of benchmark perylene monomers PMI-2, PMI(OR), and PMI(OR)₃' in toluene at room temperature.

mirror image to the absorption manifold (Figure 2, dashed). The (0,0), (0,1), (0,2), and (0,3) emission features for PMI-2 are at approximately 530, 570, 617, and 680 nm, respectively. In analogy to the absorption spectrum, the fluorescence spectrum red shifts upon incorporation of 4-*tert*-butylphenoxy substituents. The origin fluorescence band of PMI-2 at 529 nm moves to 567 nm for PMI(OR) and 577 nm for PMI(OR)₃' (Table 2). On the other hand, the presence of solubilizing aryloxy groups does not significantly affect the fluorescence quantum yield of the perylene-monoimide dye (Table 2). The high fluorescence yields of $\Phi_f = 0.91$, 0.82, and 0.86 for PMI-2, PMI(OR), and PMI(OR)₃', respectively, indicate that the excited singlet state of each of these dyes has negligible nonradiative decay competing with the emission process. These perylene benchmark compounds also were found to display long and monophasic fluorescence lifetimes ($\tau \sim 5$ ns; Table 2). These data demonstrate that the perylene-monoimide building blocks employed in this study (bearing one or three aryloxy groups) are suitable accessory pigments for porphyrins.

(6) Photophysical Characterization of Perylene–Porphyrin Arrays. Absorption Spectroscopy. Figure 3 shows the absorption spectra of multiperylene–porphyrin arrays **14**, **15**, and **16**, along with the spectra of reference compounds porphyrin **6** and perylene **11**. There are several noteworthy points: (1) A small but systematic bathochromic shift is observed in the Soret band as the number of perylenes is increased, with an overall shift of 8 nm upon going from an unsubstituted porphyrin to a porphyrin bearing eight perylenes. A similar effect was

(34) Gosztola, D.; Niemczyk, M. P.; Wasielewski, M. R. *J. Am. Chem. Soc.* **1998**, *120*, 5118–5119.

(35) Holtrup, F. O.; Müller, G. R. J.; Quante, H.; De Feyter, S.; DeSchryver, F. C.; Müllen, K. *Chem.–Eur. J.* **1997**, *3*, 219–225.

TABLE 3. Absorption and Fluorescence Properties of Perylene–Porphyrin Arrays and Reference Porphyrins

compound	no. of perylene pigments	λ_{\max}^a (nm)	$\epsilon_{\text{perylene}}/\epsilon_{\text{Soret}}^b$ (%)	Φ_f^c		τ^d (ns)	
				toluene	PhCN	toluene	PhCN
ZnTPP	0	423	<i>e</i>	0.033 ^f	0.050	2.1 ^g	1.9
ZnTMP ^h	0	423	<i>e</i>	0.039 ⁱ		2.4 ^j	1.8
ZnU ^k	0	423	<i>e</i>	0.034 ^l	0.050 ^m	2.4 ⁿ	2.0 ^o
9	0	424	<i>e</i>	0.034	0.041	2.2	2.1
4	2	423, 509, 541	16	0.028	0.013		
7	2	424, 511, 544	15	0.036	0.045		
14	2	424, 508, 543	16	0.036	0.047		
15	4	426, 508, 538	40	0.044	0.070	2.1	2.0
16	8	431, 507, 533	73	0.050	0.050	2.1	1.7

^a Absorption maxima in toluene at room temperature. ^b $\epsilon_{\text{perylene}} = \epsilon_{\max}$ from 509 to 544 nm in toluene. ^c Fluorescence emission yields ($\pm 10\%$) were determined upon excitation (423 nm) of solutions in toluene or benzonitrile at room temperature by ratioing to that of ZnTPP in toluene. A small fraction of the observed emission stems from the perylene. ^d Fluorescence lifetime (± 0.2 ns). ^e Not applicable. ^f Reference 37. ^g Values in the range 2.0–2.1 ns were determined here and in ref 38. ^h ZnTMP is zinc(II) tetramesitylporphyrin. ⁱ Reference 39. ^j Average of 2.3 ns found here and 2.4 and 2.5 ns found in ref 39. ^k ZnU is zinc(II) 5-[4-[2-(trimethylsilyl)ethynyl]phenyl]-10,15,20-trimesitylporphyrin. ^l References 38 and 39a. ^m Values in the range 0.04–0.06 with an average of 0.05 have been measured for this compound in a number of polar coordinating solvents. ⁿ Agrees with the values 2.4 and 2.5 ns reported in ref 38. ^o Values in the range 2.3–2.6 ns are reported in ref 38 for other polar coordinating solvents, including acetonitrile.

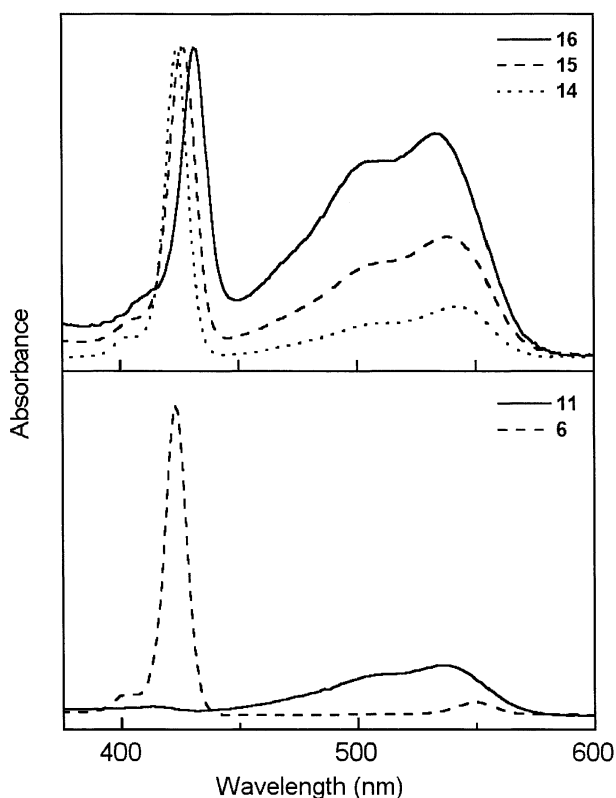


FIGURE 3. Absorption spectra for perylene–porphyrin arrays **14**, **15**, and **16**, reference porphyrin **6**, and perylene **11**. All spectra were collected at room temperature in toluene.

noted in the architecturally similar array bearing eight boron-dipyrrin dyes.⁵ (2) The absorption due to the perylene in the arrays increases essentially linearly upon going from two to four to eight perylenes (on the basis of the normalized porphyrin Soret band). (3) The absorption spectrum in the visible region of each perylene–porphyrin array is well approximated by the sum of the spectra of the component parts. This observation is indicative of the relatively weak electronic coupling between the perylenes and porphyrin. The absorption properties of the arrays are summarized in Table 3.

Fluorescence Spectroscopy. Each perylene–porphyrin array (**4**, **7**, **14–16**) and porphyrin reference

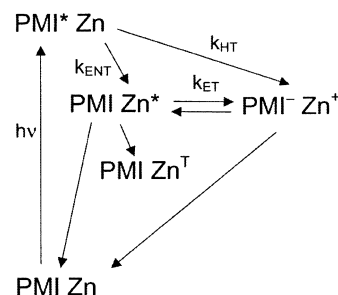


FIGURE 4. Schematic state diagram for the key processes open to the perylene (PMI) and porphyrin (Zn) in the arrays. These processes are energy transfer (ENT), hole transfer (HT), and electron transfer (ET).

compound **9** were analyzed by fluorescence emission spectroscopy. Measurements were performed in both toluene and benzonitrile to garner information as to the excited-state behavior of these systems in nonpolar and polar media, respectively. To facilitate the presentation of the photophysical data, in Figure 4, we depict the most likely energy-transfer (ENT), hole-transfer (HT), and electron-transfer (ET) processes in the perylene–porphyrin arrays that compete with the emissive and nonradiative decay pathways operative in the isolated chromophores.^{7–12}

Excitation of a perylene–porphyrin array at 490 nm, where the perylene dye absorbs preferentially, results in an emission characteristic of both the perylene (500–700 nm) and the zinc porphyrin [Q(0,0) and Q(0,1) bands at 595 and 650 nm, respectively]. The yield of emission from the perylene is diminished at least 30-fold from that of the benchmark perylene monomer. These results are consistent with efficient energy transfer to the porphyrin. In each case, the observation of a significant level of emission from the perylene and from the porphyrin reflects the fact that the inherent quantum yield of fluorescence for the perylene donor is very high ($\Phi_f = 0.8–0.9$; Table 2),¹² whereas that for the zinc porphyrin is relatively low ($\Phi_f = 0.03–0.05$, depending on substituents and solvent^{8,36–39}). The energy-transfer yields in

(36) Seybold, P. G.; Gouterman, M. *J. Mol. Spectrosc.* **1969**, *31*, 1–13.

the multiperylene–porphyrin arrays are determined more accurately from the time-resolved measurements described below.

The fluorescence yield of the zinc porphyrin in each array also was examined ($\lambda_{\text{exc}} = 423 \text{ nm}$) in order to identify any quenching interactions due to the presence of the appended perylene dyes. Quantum yield measurements were performed in both toluene and benzonitrile because the rates of charge-transfer quenching processes are influenced by the effect of the solvent polarity on the free energies of charge-separated product states, such as $\text{PMI}^- \text{Zn}^+$ (Figure 4). In toluene, each perylene–porphyrin array has a fluorescence yield $\Phi_f = 0.028\text{--}0.050$. Up to 10% of the emission could be due to residual perylene fluorescence elicited by direct excitation of this chromophore. Accordingly, the fluorescence from the porphyrin in the array is comparable to or slightly greater than that for a given zinc porphyrin reference monomer^{8,36–39} (Table 3). Similar analysis for each array (except **4**) in benzonitrile also results in a fluorescence yield ($\Phi_f = 0.045\text{--}0.070$) generally comparable to those for the reference porphyrins in this solvent or others that can coordinate to the central zinc ion. The slightly increased fluorescence yields and (less) slightly reduced excited-singlet-state lifetimes of the zinc porphyrins in metal-coordinating solvents can be traced to an increased radiative rate constant k_f . The increased k_f is also manifested in the intensity of the origin transition in the optical absorption and emission spectra. Increased k_f values are also often observed, depending on the substituents (ethyne, mesityl, halogen, etc.) on the aryl rings of the porphyrin. In general, these effects derive from modulation of the porphyrin frontier molecular orbitals and, thus, the wavefunction of the lowest excited singlet state.^{8,10,38,39} In addition, steric–electronic effects of the multiple perylenes present in **15** and **16** may slightly alter the electronic interactions involving the ethyne-containing aryl groups and the porphyrin macrocycle, causing a small increase in the radiative rate constant k_f and, thus, the fluorescence yield. However, such effects represent a relatively minor perturbation on the properties of the excited porphyrin in these architectures.

Analysis of the fluorescence yields using standard methods^{8,38,39} suggests that there is virtually no quenching or, at worst, only modest quenching of the excited porphyrin due to the presence of multiple perylene accessory pigments in the arrays. The only clear exception based on the emission yields is **4** in benzonitrile, where the significantly reduced fluorescence likely stems from competing electron transfer (forming $\text{PMI}^- \text{Zn}^+$; Figure 4) derived from the shorter perylene–porphyrin distance compared to those of the other arrays. Compound **4** is unique in that the perylenes are attached at the 2,6-positions rather than the 3,5-positions of the

meso-aryl ring of the porphyrin, reducing the distance from the Zn atom of the porphyrin to the middle of the central benzenoid ring of the perylene from 17.5 to 11.1 Å.

We also measured the fluorescence lifetimes of the largest arrays (and several reference compounds) in both toluene and benzonitrile in order to obtain a second measure of the extent to which the excited porphyrin may be affected by the presence of multiple appended accessory pigments. These excited-state lifetimes (all $\pm 0.2 \text{ ns}$) are given in Table 3. The lifetimes for **9** (2.2 ns), **15** (2.1 ns), and **16** (2.1 ns) in toluene are virtually the same. The values for **9** (2.1 ns) and **15** (2.0 ns) in benzonitrile may be slightly shorter than those in toluene, consistent with the expected slightly increased k_f due to metal coordination. The lifetime for **16** in benzonitrile (1.7 ns) shows the only clear (yet modest) reduction in value compared to that of the reference porphyrin. Analysis of the lifetimes for **15** and **9** using standard methods^{8,38,39} indicates that there is little quenching of the excited zinc porphyrin in **15** due to the presence of the four appended perylenes in either toluene or benzonitrile. A similar analysis for **16** indicates little effect on the porphyrin due to the presence of eight perylenes in toluene. For example, the quenching yield for **15** and **16** in toluene is $\Phi_Q = (1 - 2.1 \text{ ns} / 2.2 \text{ ns}) \times 100 \sim 5\%$ and that for **15** in benzonitrile is $\Phi_Q = (1 - 2.0 \text{ ns} / 2.1 \text{ ns}) \times 100 \sim 5\%$; however, in each of these cases, the quenching yield could be $\sim 10\%$ given experimental uncertainty. The eight perylenes in **16** give a somewhat larger (yet still modest) quenching of the excited porphyrin in benzonitrile ($\Phi_Q = (1 - 1.7 \text{ ns} / 2.1 \text{ ns}) \times 100 \sim 20\%$). In each case, the quenching is likely due to $\text{PMI} \text{Zn}^* \rightarrow \text{PMI}^- \text{Zn}^+$ electron transfer, as illustrated in Figure 4.^{8–12}

Time-Resolved Absorption Spectroscopy. Arrays **15** and **16** were examined by time-resolved absorption spectroscopy in order to determine the rate and yield of perylene-to-porphyrin energy transfer and to further assess the contribution of any non-energy-transfer processes to the observed photodynamics. Perylene–porphyrin arrays **15** and **16** in toluene or benzonitrile were excited with a 130-fs flash at 485 nm, which is primarily absorbed by perylene. The excitation-light intensity was attenuated to avoid pumping more than one of the four perylenes in **15** or eight perylenes in **16**. Representative spectral and kinetic data for **15** in toluene are shown in Figure 5, and some of the data are reproduced in Figure 6B.

The transient absorption difference spectrum immediately after excitation of **15** in toluene shows essentially exclusively characteristics of the excited perylene PMI^* (0.5 ps spectrum in Figure 5A, dotted). One of the two main features is a broad trough at $\sim 530 \text{ nm}$ that contains bleaching of the $\text{PMI} (0,0)$ ground-state absorption band together with PMI^* excited-state stimulated emission.⁴⁰ The second main feature is a broad PMI^* excited-state absorption with a maximum at $\sim 700 \text{ nm}$. The PMI^* spectrum for **15** is similar to those that we have observed previously for excited perylene-monoidide dyes in isolation and in dyads with porphyrins, with the

(37) Gouterman, M. In *The Porphyrins*; Dolphin, D., Ed.; Academic Press: New York, 1978; Vol. III, pp 1–165.

(38) (a) Hsiao, J.-S.; Krueger, B. P.; Wagner, R. W.; Johnson, T. E.; Delaney, J. K.; Mauzerall, D. C.; Fleming, G. R.; Lindsey, J. S.; Bocian, D. F.; Donohoe, R. J. *J. Am. Chem. Soc.* **1996**, *118*, 11181–11193. (b) Li, F.; Gentemann, S.; Kalsbeck, W. A.; Seth, J.; Lindsey, J. S.; Holten, D.; Bocian, D. F. *J. Mater. Chem.* **1997**, *7*, 1245–1262.

(39) (a) Yang, S. I.; Seth, J.; Strachan, J.-P.; Gentemann, S.; Kim, D.; Holten, D.; Lindsey, J. S.; Bocian, D. F. *J. Porphyrins Phthalocyanines* **1999**, *3*, 117–147. (b) Yang, S. I.; Lammi, R. K.; Seth, J.; Riggs, J. A.; Arai, T.; Kim, D.; Bocian, D. F.; Holten, D.; Lindsey, J. S. *J. Phys. Chem. B* **1998**, *102*, 9426–9436.

(40) Emission from the excited chromophore is stimulated by the white-light probe pulse, appears as negative ΔA in the absorption difference spectra, and occurs at approximately the same wavelengths as the spontaneous emission.

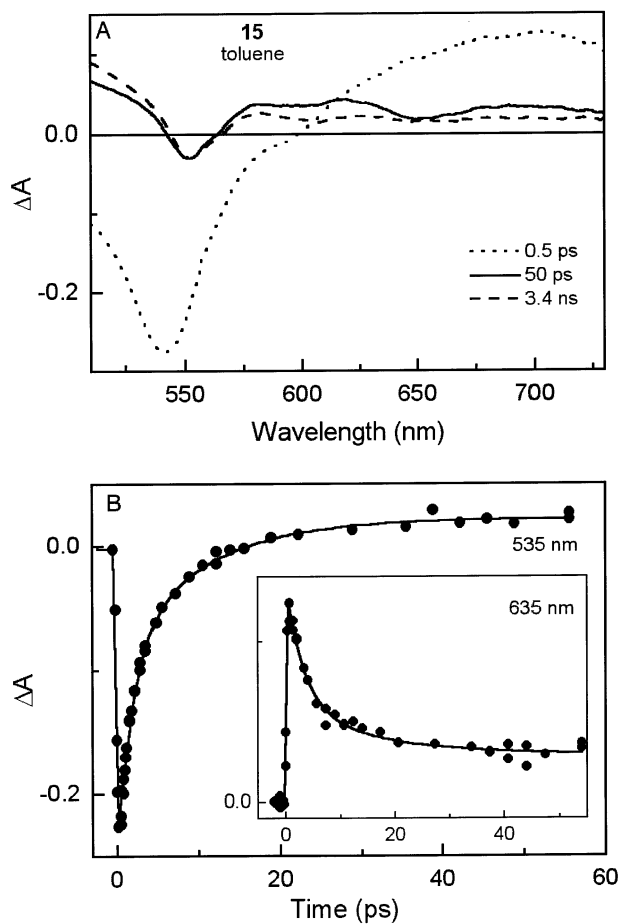


FIGURE 5. Time-resolved absorption spectra (A) and kinetic profiles (B) for perylene–porphyrin array **15** at room temperature in toluene. The fits to the kinetic data in part B are to the instrument response and dual-exponential decays plus a constant, giving time constants of 2.7 and 9.5 ps (535 nm, main figure) and 3.3 and 12 ps (635 nm, inset). The amplitude-weighted average value from these and other wavelengths is 3.5 ps. The PMI* spectrum was constructed by concatenating several spectra at successive delay times, owing to the distortions in the raw difference spectra of this rapidly decaying state due to the dispersion in the arrival times at the sample of the different wavelengths in the probe pulse.

following caveat.^{10–12} Like the ground-state absorption and fluorescence spectra described above, the PMI* excited-state optical characteristics in **15** are affected by the presence of the three aryloxy groups on each perylene. In particular, these groups broaden and red-shift all the features compared to the cases of the arrays containing perylene-monoimides with fewer or no solubilizing substituents.

The PMI* spectrum decays rapidly, as is seen from the representative kinetic data and fits in Figure 5B. The figure shows decay of the PMI ground-state bleaching at 535 nm (main panel) and PMI* excited-state absorption at 635 nm (inset). At each wavelength, the data are best fit with a dual-exponential function.⁴¹ Nevertheless, the kinetic data across the spectral region shown in Figure 5A when taken as a whole are reasonably represented by an average PMI* lifetime of ~3.5 ps. This lifetime is about 1000-fold shorter than the PMI* lifetime of 5 ns for reference perylene PMI(OR)₃' (Table 2). This signifi-

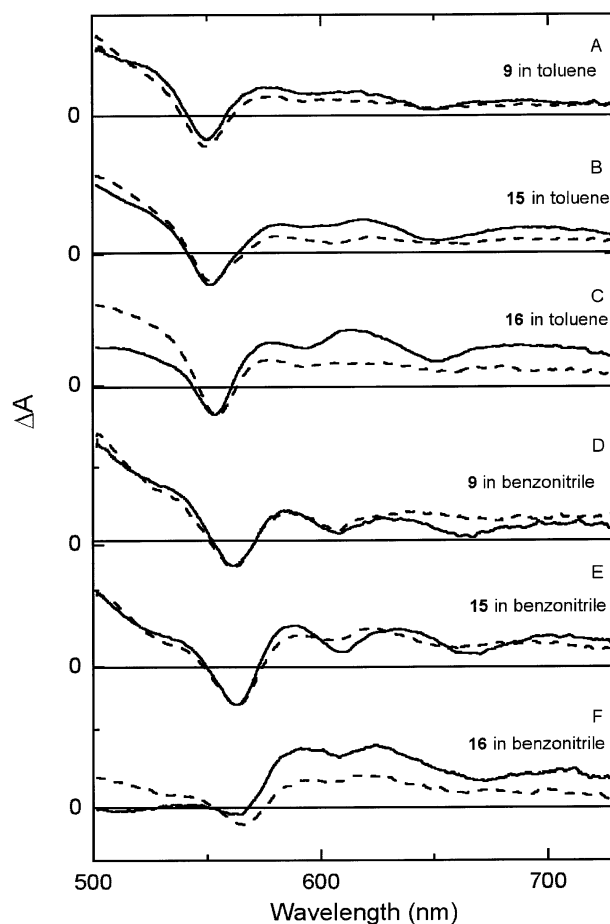


FIGURE 6. Time-resolved absorption spectra for porphyrin **9** and perylene–porphyrin arrays **15** and **16** in toluene and benzonitrile. The spectra for **15** in panel B are reproduced from Figure 5. The solid spectra are at pump–probe delay times of 1 ps (**9**) or 50 ps (**15**, **16**), and the dashed spectra are at 3.4 ns.

cant difference indicates the involvement of at least one process open to PMI* in the array that is not operable in the isolated chromophore. On the basis of our previous work with perylene–porphyrin arrays,^{7–12} the most likely processes are PMI* Zn → PMI Zn* energy transfer and PMI* Zn → PMI⁻ Zn⁺ hole transfer (Figure 4).

The spectral evolution for **15** in toluene indicates that the PMI* decay occurs predominantly (>90%) by the energy-transfer channel. In particular, by ~50 ps, the PMI* spectrum has been fully replaced by the spectrum of the excited zinc porphyrin (Figures 5A and 6B, solid). The Zn* spectrum shows all the expected features, which

(41) The time-evolution of PMI* in either **15** or **16** in either toluene or benzonitrile indicates the presence of two components whose time constants and relative contributions to the spectra depend on detection wavelength. The major component generally has a lifetime of 2–5 ps, and the second component has that of 6–16 ps. The second component is much less prominent for either array in benzonitrile as compared to toluene. From analysis across the spectral region shown in Figure 6, the amplitude-weighted average time constants are 3.9 ps for **15** in toluene, 3.5 ps for **16** in toluene, 3.4 ps for **15** in benzonitrile, and 2.7 ps for **16** in benzonitrile. Considering the complexities of the decays, we used a mean PMI* lifetime of 3.5 ps in each case. The presence of two components indicates that the observed PMI* dynamics involve (at least) two excited-state forms (vibrational, conformational, electronic) along with relevant relaxation processes. These effects are more prominent with aryloxy-substituted perylenes.¹²

are also seen in the spectra for the isolated porphyrin reference compound **9** in toluene (compare Figure 6A and B, solid). These Zn^* features include Q(1,0) bleaching at ~ 550 nm, combined Q(0,0) bleaching and stimulated emission at 595 nm, and Q(0,1) stimulated emission at 650 nm.⁴⁰ All of these features are embedded on a relatively broad excited-state absorption that increases in strength in the blue-green region.

Over the next several nanoseconds (and to the ~ 3.5 -ns limit of the transient absorption spectrometer), the Zn^* stimulated emission decays away (e.g., the feature at 650 nm), with comparatively small changes in the ground-state bleaching when referenced to the broad excited-state absorption. This spectral evolution seen for array **15** in toluene (Figures 5A and 6B, dashed) is also observed for reference porphyrin **9** in the same solvent (Figure 6A, dashed). These spectral changes are expected for formation of the porphyrin excited triplet state (Zn^{T}) via intersystem crossing in high yield⁴² ($>80\%$). This triplet-state formation occurs with the relatively long (~ 2 ns) Zn^* lifetime measured for array **15** and porphyrin **9** via fluorescence decay. Consistent with the emission yields and lifetimes, the transient absorption spectra for **15** in toluene reveal no significant ($\leq 10\%$) formation of charge-separated states such as $\text{PMI}^- \text{Zn}^+$ from either PMI^* (by hole transfer) or Zn^* (by electron transfer). The production of a charge-separated state would have given PMI ground-state bleaching (and PMI^- absorption) either in parallel with Zn^* formation or during Zn^* decay, which would have distorted the porphyrin excited-state spectra in array **15** from those expected and observed for the isolated reference porphyrin.^{8–12}

The time-resolved absorption spectra described above for array **15** in toluene (Figures 5 and 6B) and porphyrin monomer **9** in toluene (Figure 6A) provide a framework for assessing the extent to which hole/electron-transfer reactions supplement the primary energy-transfer processes for **16** in toluene and for **15** and **16** in benzonitrile. To this end, Figure 6C–F shows key transient absorption spectra for the latter three cases along with data for **9** in benzonitrile. All the data in Figure 6 were acquired and are presented so that the spectral shapes and amplitudes can be compared among the different compounds/solvents. Furthermore, the amplitude and general shape of the subpicosecond PMI^* spectrum for **15** in toluene (Figure 5A, dotted) are relevant not only for the data at longer times reproduced for that compound in Figure 6B but also for the spectra at longer times for **16** in toluene and **15** and **16** in benzonitrile presented in Figure 6 (50 ps, solid; 3.4 ns, dashed). In analogy to the case of **15** in toluene, the PMI^* decay profiles for **16** in toluene and for **15** and **16** in benzonitrile are complex (more so in toluene) but are reasonably described by an average time constant of 3.5 ps.⁴¹ The most significant differences that occur for arrays/solvents are seen in the spectra (and states) formed from PMI^* decay, and subsequently from Zn^* decay, as described below.

(42) (a) Gradyushko, A. T.; Sevchenko, A. N.; Solovyov, K. N.; Tsvirko, M. P. *Photochem. Photobiol.* **1970**, *11*, 387–400. (b) Hurley, J. K.; Sinai, N.; Linschitz, H. *Photochem. Photobiol.* **1983**, *38*, 9–14. (c) Kajii, Y.; Obi, K.; Tanaka, I.; Tobita, S. *Chem. Phys. Lett.* **1984**, *111*, 347–349. (d) Kikuchi, K.; Kurabayashi, Y.; Kokubun, H.; Kaizu, Y.; Kobayashi, H. *J. Photochem. Photobiol., A* **1988**, *45*, 261–263. (e) Bonnett, R. D.; McGarvey, D.; Harriman, A.; Land, E. J.; Truscott, T. G.; Winfield, U. J. *Photochem. Photobiol.* **1988**, *48*, 271–276.

Unlike the spectrum at 50 ps for **15** in toluene that was assigned primarily ($>90\%$) to Zn^* , the spectrum at this time delay for **16** in toluene has characteristics of $\text{PMI}^- \text{Zn}^+$ in addition to the dominant contribution of Zn^* (both formed from PMI^* ; Figure 4). The formation of the charge-separated state in the latter array is deduced from several characteristics of the transient difference spectra. The primary signature is a diminished amplitude of the transient absorption due to Zn^* between 500 and 540 nm for **16** in toluene relative to array **15** or porphyrin **9** in this solvent (compare solid spectra in Figure 6A–C). The diminished blue-green (positive) transient absorption for **16** derives primarily from the compensating (negative) bleaching of the modestly strong ground-state absorption of PMI in this region (Figure 2C) that occurs when state $\text{PMI}^- \text{Zn}^+$ forms (but which is not present for Zn^*).

To estimate the yield of the hole-transfer process, the reasonable assumption is made that the PMI bleach in the blue-green region for $\text{PMI}^- \text{Zn}^+$ is approximately the same as that for PMI^* . This analysis takes into account the estimated contribution of PMI^* -stimulated emission in the 500–540-nm region for state PMI^* and ignores possible small differences in the excited-state absorption of this state and $\text{PMI}^- \text{Zn}^+$ in this region.^{10–12} Using these assumptions along with the 0.5-ps PMI^* spectrum for **15** in toluene in Figure 5A (dotted) and the companion 50-ps Zn^* spectrum (Figure 5A and 6B, solid) as guides, it is estimated that the 50-ps spectrum for **16** in toluene (Figure 6C, solid) contains $\sim 10\%$ $\text{PMI}^- \text{Zn}^+$ and $\sim 90\%$ Zn^* . Such a small amount of the charge-separated state is discernible because of the “pulling down” effect on the Zn^* transient absorption between 500 and 540 nm caused by even a small amount of perylene bleaching when one considers the much larger inherent amplitude of the latter feature compared to the former (e.g., Figure 5A dotted and solid). In addition to the altered spectral characteristics in the 500–540-nm region, another indication that $\text{PMI}^- \text{Zn}^+$ contributes to the 50-ps spectrum for **16** in toluene is increased transient absorption in the vicinity of 630 nm compared to that of array **15** or porphyrin **9** in this solvent (Figure 6A–C, solid). We have previously found that the anions of the appropriate perylene-monoimide dyes have prominent transient absorption bands centered in the 620–650-nm region.^{10–12}

The small amount of $\text{PMI}^- \text{Zn}^+$ formed from PMI^* for **16** in toluene appears to largely decay by the 3.4-ns limit of the transient absorption experiment, given that the spectra at this time are very similar to those for array **15** and porphyrin **9** in this solvent (Figure 5), all of which have been assigned to Zn^{T} . This observation is consistent with the finding of similar porphyrin fluorescence lifetimes for these three compounds in toluene (Table 3), which indicates that the decay characteristics of Zn^* for **16** in toluene are comparable (within $\sim 10\%$) to those of the isolated chromophore.

Similar analyses can be performed for **15**, **16**, and reference porphyrin **9** in benzonitrile (Figure 6D–F). In short, the transient difference spectra for **9** and **15** in benzonitrile (Figure 6D and E) are similar to one another, just as was found in comparing the spectra for these two compounds in toluene (Figure 6A and B). The only difference is in the positions and relative amplitudes of the bleaching and stimulated-emission features in ben-

zonitrile versus toluene (as expected from the comparable changes in the static optical spectra due to coordination of the benzonitrile solvent molecules to the central zinc ion of the porphyrin). Thus, **15** in benzonitrile has a rapid PMI* decay (~ 3.5 ps)⁴¹ that occurs primarily ($\geq 90\%$) by energy transfer to the porphyrin, and subsequently, Zn* decays with characteristics comparable (within $\sim 10\%$) to those for the isolated chromophore.

The spectrum at 50 ps for array **16** in benzonitrile (Figure 6F, solid) suggests that PMI* decays in part by hole transfer to form PMI⁻ Zn⁺. In benzonitrile, the Zn* absorption between 500 and 540 nm is “pulled down” even further by the opposing perylene bleaching than it is in toluene, indicating that the amount of the charge-separated state has increased in yield from $\sim 10\%$ in toluene to $\sim 20\%$ in benzonitrile. At 3.4 ns (Figure 6F, dashed), the Zn^T spectrum in benzonitrile is compromised by apparent formation of some PMI⁻ Zn⁺ via electron transfer from Zn* back to the perylene. On the basis of the fluorescence lifetime data presented above (Table 3), we estimated this Zn* electron-transfer quenching to have a yield of $\sim 20\%$, which is consistent with the transient absorption spectra.

Summary of Excited-State Dynamics. The photo-physical data for arrays containing two (**7** and **14**), four (**15**), and eight (**16**) perylenes attached at the meta-positions of the porphyrin indicate that these are excellent light-harvesting motifs, with the optimum being four perylenes. The collective data are internally consistent and indicate that the yield of PMI* Zn \rightarrow PMI Zn* energy transfer is $> 90\%$ for arrays with two or four perylenes in toluene or benzonitrile, $\sim 90\%$ for **16** in toluene, and $\sim 80\%$ for **16** in benzonitrile. The remaining fraction of the PMI* decay in each case primarily involves PMI* Zn \rightarrow PMI⁻ Zn⁺ hole transfer (Figure 4), which has a yield of at most $\sim 20\%$ (for **16** in benzonitrile). Regarding these results, we should note that, in principle, the same yield for perylene-to-porphyrin energy transfer should be found for all the analogous arrays (**7**, **14**, **15**, **16**) in a given solvent, since only one perylene in each array should be excited at any time and each perylene should behave independently in energy (or hole) transfer to the central porphyrin. The energy-transfer yield will increase slightly for a given array in benzonitrile as compared to toluene because of stabilization of the PMI⁻ Zn⁺ state in the polar solvent. These expectations are generally borne out by the results. The only apparent deviation is a small increase in the hole-transfer yield for **16** as compared to **15** (especially in benzonitrile). This finding may derive from small (structural) effects of the eight perylenes in **16** on the electronic interactions with the porphyrin, as noted earlier regarding the static optical spectra, or from the assumptions made in analyzing the time-resolved optical spectra that may lead to overestimates of the hole-transfer yields. Nevertheless, deviations from the expectation of similar perylene-to-porphyrin energy-transfer yields among the arrays are small. Furthermore, the collective results indicate that energy transfer to the porphyrin dominates the decay of PMI* in all the arrays.

For each dyad, the rate constants for PMI* energy and hole transfers (Figure 4) can be estimated from the time-resolved data using standard analysis.^{8,38,39} For example, the average PMI* lifetime of $\tau \sim 3.5$ ps⁴¹ for **15** in toluene (like the other arrays and solvents) is considerably

shorter than $\tau^m = 5$ ns in the isolated perylene PMI(OR)₃' (Table 2). These data give a rate constant for the quenching of PMI* by the porphyrin of $k_Q = (1/\tau - 1/\tau^m) \sim (3.5 \text{ ps})^{-1}$. On the basis of the yields estimated above, the rate constant for PMI* Zn \rightarrow PMI Zn* energy transfer is $k_{\text{ENT}} = 0.95 \times (3.5 \text{ ps})^{-1} \sim (3.7 \text{ ps})^{-1}$ for **15** in toluene. The corresponding microscopic rate constant for hole transfer is $k_{\text{HT}} = 0.05 \times (3.5 \text{ ps})^{-1} \sim (70 \text{ ps})^{-1}$.

Once the excited porphyrin is formed (by energy transfer from perylene or direct excitation), Zn* decays with characteristics (lifetime, emission yield) comparable (within $\sim 10\%$) to those operable in the isolated porphyrin (Figure 4). Within the series of analogous arrays **7**, **14**, **15**, and **16**, porphyrin quenching rises above the $\sim 10\%$ level only for **16** in benzonitrile, for which Zn* decays $\sim 20\%$ via electron transfer back to PMI with an overall rate constant of $0.2 \times (2.1 \text{ ns})^{-1} \sim (10 \text{ ns})^{-1}$. Since the porphyrin can transfer an electron to any one of the eight perylenes in **16**, the microscopic rate constant for each process is $(10 \text{ ns})^{-1}/8 = (80 \text{ ns})^{-1}$. Thus, electron transfer is significantly slower than the normal routes (intersystem crossing, internal conversion, fluorescence) operable in the isolated porphyrin. These results suggest that the PMI⁻ Zn⁺ charge-separated state lies above Zn* (but below PMI*) in toluene and moves close to or possibly slightly below Zn* in benzonitrile because of solvent stabilization.

Thus, the modest increase in the PMI Zn* \rightarrow PMI⁻ Zn⁺ electron-transfer yield to $\sim 20\%$ for **16** in benzonitrile as compared to $\sim 10\%$ in toluene can be understood by a solvent-polarity effect on the rate, as we have found for other perylene–porphyrin arrays.^{9,11,12} In turn, a small increase in the overall Zn* electron-transfer yield for **16** versus **15** derives from the presence of twice as many perylenes in the former array. The observations are consistent with the microscopic energy-transfer rate constant being the same for both arrays (and for the arrays containing fewer perylenes) in a given solvent. However, as noted earlier for the decay of PMI*, the perylene–porphyrin interactions may be perturbed slightly with an increasing number of perylenes because of structural–electronic effects, although these effects appear to be relatively small.

In summary, the extensive blue-green absorption of the eight perylenes appended to the porphyrin in **16** affords a suitable light-harvesting system that has relatively minor competing charge-transfer quenching of the excited perylene in nonpolar solvents and modest competing quenching of both the perylene and porphyrin in highly polar media. Charge-transfer quenching is even less for **15**, for which the four perylenes still give substantial absorption complementary to that of the porphyrin to make an excellent light-harvesting motif in both polar and nonpolar media.

(7) Effective Accessory Pigments. The perylene-monoimide dyes examined herein appear to be ideal for use as accessory pigments with porphyrins. The perylene dyes provide the following attributes: (1) absorption in the trough between the porphyrin B and Q bands; (2) rapid and efficient energy transfer to the porphyrin; (3) limited or no competing electron-transfer quenching processes with the photoexcited porphyrin in polar or nonpolar solvents; (4) long, monophasic excited-state lifetime, high fluorescence yield, and very low yield of

intersystem crossing; (5) compatibility with a building block synthesis; (6) amenability to architectures with multiple accessory pigments; and (7) high solubility and nonpolar nature, affording facile purification. Very few classes of dyes meet this set of criteria.⁴³ For example, xanthenes or cyanine dyes provide superior laser dyes and/or biolabels but are difficult to purify given their intrinsic charge. Carotenoids absorb strongly but have an exquisitely short excited-state lifetime requiring very close proximity to the porphyrin for efficient energy transfer. Boron-dipyrrin dyes have two excited-state conformers with short lifetimes, cause quenching of the photoexcited porphyrin in polar solvents, and, in addition, present purification challenges upon incorporation in multipigment arrays because of their intrinsic polarity. The perylene-monoimides provide about 2.5-times the integrated absorption ($\epsilon_{\text{max}} \times \text{fwhm}$) of that of boron-dipyrrin dyes, which we have used previously for light-harvesting applications. All factors considered, the perylene and linker motifs examined herein are very well suited for use with porphyrins in light-harvesting architectures.

Conclusion

Several new perylene–porphyrin light-harvesting arrays have been synthesized and characterized in order to identify suitable multiperylene–porphyrin motifs for use in larger light-harvesting arrays. The preparation of the arrays followed two synthetic strategies: (1) an ethynylporphyrin building block was coupled with a bromoperylene (affording arrays **4** and **7**), and (2) a perylene–aldehyde was employed in a porphyrin-forming reaction (affording arrays **14**–**16**). All arrays examined exhibit virtually quantitative ($\geq 90\%$) excited-state energy transfer from perylene to porphyrin except for the array with eight perylenes in polar media, which gave a 20% loss due to competing charge-transfer quenching. The arrays with tris(aryloxy)perylene-monoimide dyes positioned at the 3,5-positions of one, two, or four aryl rings of the porphyrin have high solubility and unperturbed porphyrin fluorescence lifetimes and yields in nonpolar (toluene) solvents and, in most cases, in polar (benzonitrile) solvents as well. Only with eight perylenes per porphyrin in benzonitrile is there a clear ($> 10\%$) quenching of the excited porphyrin, and again at a modest level of $\sim 20\%$. By comparison, the arrays with perylene-monoimide dyes positioned at the 2,6-positions provide a more compact geometry but are synthesized in lower yields and also are less suited for light-harvesting applications in polar media.

Overall, the array containing four perylenes attached at the 3,5-positions of two *trans*-aryl rings of the porphyrin provides the optimal characteristics in both polar and nonpolar media in terms of light harvesting with little if any ($\leq 10\%$) deleterious charge-transfer quenching of either the excited perylene or porphyrin. This motif leaves the other two aryl rings of the porphyrin free for attaching synthetic handles. These functionalities can be

used in a building block approach to construct light-harvesting rods consisting of a central chain of porphyrins decorated by closely packed perylene accessory pigments. The preparation and study of such architectures based on the results obtained in the present paper are now underway.

Experimental Section

General. ¹H (300 or 400 MHz) and ¹³C (75 MHz) NMR spectra were recorded in CDCl₃ unless noted otherwise. Mass spectra of porphyrins and perylene–porphyrin arrays were obtained by high-resolution fast atom bombardment (FABMS) and/or by laser desorption mass spectrometry (LDMS)⁴⁴ or matrix-assisted LDMS (MALDI-MS) using the matrix dithranol. Absorption and emission spectra were collected in toluene unless noted otherwise. Elemental analyses were performed by Atlantic Microlab, Inc. Melting points are uncorrected. Silica gel (40 μm average particle size) and alumina (80–200 mesh) were used for column chromatography. Preparative SEC was performed using BioRad Bio-Beads SX-1 (200–400 mesh) beads. Analytical SEC was performed using an HPLC (column size = 1000 Å; flow rate = 0.800 mL/min; solvent = THF; quantitation at 420 and 510 nm; reference at 670 nm; oven temperature at 25 °C).⁴⁵ All Pd-mediated reactions were performed using a Schlenk line. The conditions for Sonogashira reactions with porphyrins use tris(dibenzylideneacetone)-dipalladium(0) (Pd₂(dba)₃) and P(*o*-tol)₃ in the absence of any copper reagents.²⁶ Palladium insertion and transmetalation have not been observed with these conditions. Toluene and triethylamine were freshly distilled from CaH₂ and sparged of oxygen prior to use. Chloroform contained 0.8% ethanol as a stabilizer. PC Model for Windows 7.50.00 (Serena Software, Inc.) was used to generate the space-filling model in Figure 1 and to calculate intramolecular distances.

Noncommercial Compounds. Aldehyde **5**;⁵ 5-mesityldipyrrromethane (**8**);²⁸ and perylenes PMI-1³¹ and PMI-2³² were prepared as described in the literature. The syntheses of perylenes **3**, **10**, PMI(OR), and **11** will be described elsewhere.¹²

Optical Spectroscopy. Absorption spectra (HP 8453, Cary 3) and fluorescence spectra (Spex FluoroMax) were collected as described previously using nondegassed solutions (typically $< 1 \times 10^{-5}$ M).³⁹ Fluorescence quantum yields were determined by ratioing the integrated corrected emission spectrum of the sample to that of ZnTPP (0.033)³⁷ or *N,N*-bis(2,5-di-*tert*-butylphenyl)-3,4:9,10-perylenedicarboximide (0.97).¹⁵ Transient absorption data were obtained at room temperature as described elsewhere.⁴⁶ Samples (~ 0.1 to 0.2 mM in toluene or benzonitrile) in 2-mm path length cuvettes were excited at 10 Hz with 130-fs pump pulses (20–35 μJ at 475–490 nm) and probed with white light pulses of comparable duration.

2,6-Bis[2-(trimethylsilyl)ethynyl]benzaldehyde (1). Following the method described by Buchwald and Fu,²² samples of 2,6-dichlorobenzaldehyde (3.56 g, 20.4 mmol), Pd(PhCN)₂Cl₂ (468 mg, 1.22 mmol), and CuI (155 mg, 814 μmol) were placed in a Schlenk flask. Diisopropylamine (6.7 mL), dioxane (30 mL), and P(*t*-Bu)₃ (494 mg, 2.44 mmol) were placed in a second Schlenk flask and sparged of oxygen for 10 min, and then the mixture was added to the first Schlenk flask. The flask was

(44) (a) Fenyó, D.; Chait, B. T.; Johnson, T. E.; Lindsey, J. S. *J. Porphyrins Phthalocyanines* **1997**, *1*, 93–99. (b) Srinivasan, N.; Haney, C. A.; Lindsey, J. S.; Zhang, W.; Chait, B. T. *J. Porphyrins Phthalocyanines* **1999**, *3*, 283–291.

(45) del Rosario Benites, M.; Johnson, T. E.; Weghorn, S.; Yu, L.; Rao, P. D.; Diers, J. R.; Yang, S. I.; Kirmaier, C.; Bocian, D. F.; Holten, D.; Lindsey, J. S. *J. Mater. Chem.* **2002**, *12*, 65–80.

(46) (a) Yang, S. I.; Li, J.; Cho, H. S.; Kim, D.; Bocian, D. F.; Holten, D.; Lindsey, J. S. *J. Mater. Chem.* **2000**, *10*, 283–296. (b) Kirmaier, C.; Holten, D. *Biochemistry* **1991**, *30*, 609–613.

(47) Böhm, A.; Helfer, W. U.S. Patent 5,808,073.

(48) Hofkens, J.; Latterini, L.; De Belder, G.; Gensch, T.; Maus, M.; Vosch, T.; Karni, Y.; Schweitzer, G.; De Schryver, F. C.; Hermann, A.; Müllen, K. *Chem. Phys. Lett.* **1999**, *304*, 1–9.

(43) (a) Wagner, R. W.; Lindsey, J. S. *Pure Appl. Chem.* **1996**, *68*, 1373–1380. (b) Wagner, R. W.; Lindsey, J. S. *Pure Appl. Chem.* **1998**, *70* (8), p. i.

placed in an oil bath heated to 70 °C. After 5 min, (trimethylsilyl)acetylene (7.19 mL, 50.9 mmol) was added and the mixture was stirred at 70 °C for 4 h. Removal of an aliquot and analysis by GC showed mono- and dicoupled products in a nearly 1:1 ratio. An additional equivalent of (trimethylsilyl)acetylene (2.9 mL, 20.4 mmol) was added. After 24 h at 70 °C, GC analysis showed no monocoupled product. The mixture was cooled to room temperature and then filtered through a pad of silica. Kugelrohr distillation (110 °C, 0.1 Torr) followed by column chromatography (silica, toluene) afforded a yellow oil (2.22 g, 37%): ¹H NMR δ 0.27 (s, 18H), 7.40–7.43 (m, 1H), 7.51 (d, *J* = 8.0 Hz, 2H), 10.63 (s, 1H); ¹³C NMR δ –0.0, 101.5, 102.5, 125.2, 132.3, 134.4, 137.2, 190.6. FABMS obsd, 299.1267; calcd, 299.1287. Anal. Calcd for C₁₇H₂₂OSi₂: C, 68.40; H, 7.43. Found: C, 67.94; H, 7.36.

Zinc(II) 5-[2,6-Bis[2-(trimethylsilyl)ethynyl]phenyl]-10,15,20-trimesitylporphyrin (2). Following a standard procedure for mixed-aldehyde condensations¹⁸ at high concentration²⁰ with BF₃·O(Et)₂–ethanol cocatalysis,¹⁹ samples of **1** (299 mg, 1.00 mmol), mesitaldehyde (445 mg, 3.00 mmol), and pyrrole (280 μL, 4.00 mmol) were condensed in CHCl₃ (56 mL) in the presence of BF₃·O(Et)₂ (129 μL, 1.02 mmol) at room temperature for 1.5 h. Then, DDQ (680 mg, 3.00 mmol) was added. After 1 h, TEA was added and the crude mixture was passed through a silica column [CHCl₃/hexanes (1:1)], affording a mixture of porphyrins. The resulting porphyrin mixture was treated with Zn(OAc)₂·2H₂O (550 mg, 2.50 mmol) in DMF (20 mL) overnight at 100 °C. Water was added to the reaction mixture, and the resulting solid was filtered. Column chromatography [silica, CH₂Cl₂/hexanes (1:1)] afforded a purple solid (10.7 mg, 1.1%): ¹H NMR δ –1.28 (s, 18H), 1.84–1.88 (m, 18H), 2.62 (m, 9H), 7.26 (m, 6H), 7.62–7.68 (m, 1H), 7.81–7.84 (m, 2H), 8.67–8.74 (m, 8H); LDMS obsd, 996.33 [M⁺]. FABMS obsd, 994.3788; calcd, 994.3805 (C₆₃H₆₂N₄Si₂Zn). λ_{abs} = 421, 548 nm; λ_{em} (λ_{ex} = 550 nm) 593, 642 nm.

Zinc(II) 5-(2,6-Diethynylphenyl)-10,15,20-trimesitylporphyrin (2). A sample of **2** (10.0 mg, 10.0 μmol) in CHCl₃/THF [5.0 mL, (1:1)] was treated with TBAF on silica gel (22.0 mg, 1.0–1.5 mmol/g) for 5 h at room temperature. The reaction mixture was washed with 10% NaHCO₃ and water and dried over Na₂SO₄. Column chromatography [silica, CHCl₃/hexanes (1:1)] afforded a purple solid (7.0 mg, 82%): ¹H NMR δ 1.84 (m, 18H), 2.08 (s, 2H), 2.62 (m, 9H), 7.25–7.26 (m, 6H), 7.69–7.74 (m, 1H), 7.90–7.93 (m, 2H), 8.67–8.74 (m, 8H); MALDI-MS obsd, 852.71 [M⁺]. FABMS obsd, 850.3042; calcd, 850.3014 (C₅₇H₄₆N₄Zn). λ_{abs} = 423, 550 nm; λ_{em} (λ_{ex} = 550 nm) 595, 644 nm.

Zinc(II) 5-[2,6-Bis[2-[4-[9-(4-*tert*-butylphenoxy)perylene-3,4-dicarboximido]-3,5-diisopropylphenyl]ethynyl]phenyl]-10,15,20-trimesitylporphyrin (4). A mixture of **2'** (7.0 mg, 8.2 μmol), **3** (14.5 mg, 20.5 μmol), Pd₂(dba)₃ (1.9 mg, 2.1 μmol), and P(*o*-tol)₃ (3.7 mg, 12 μmol) in toluene/triethylamine [2.0 mL (10:1)] was stirred at 60 °C under argon. After 2.5 h, another identical batch of catalyst was added. After 18 h, the mixture was cooled and passed through a silica column (CHCl₃). Preparative SEC (toluene) followed by column chromatography [silica, CHCl₃/hexanes (4:1)] and trituration with hexanes afforded a red solid (4.6 mg, 27%): ¹H NMR δ –0.16 (d, *J* = 6.6 Hz, 24H), 1.35 (s, 18H), 1.79–1.88 (m, 22H), 2.56, 2.60 (m, 9H), 6.61 (s, 4H), 6.88 (d, *J* = 8.1 Hz, 2H), 7.06 (d, *J* = 8.8 Hz, 4H), 7.18 (brs, 2H), 7.23 (brs, 4H), 7.42 (d, *J* = 8.8 Hz, 4H), 7.58–7.63 (m, 2H), 7.80–7.85 (m, 1H), 7.99 (d, *J* = 8.1 Hz, 2H), 8.09 (d, *J* = 8.1 Hz, 2H), 8.19–8.30 (m, 8H), 8.37 (d, *J* = 8.1 Hz, 2H), 8.41 (d, *J* = 8.1 Hz, 2H), 8.60 (d, *J* = 4.4 Hz, 2H), 8.63 (d, *J* = 4.4 Hz, 2H), 8.78 (d, *J* = 5.1 Hz, 2H), 8.87 (d, *J* = 4.4 Hz, 2H). LDMS obsd, 2110.42 [M⁺]; calcd av mass, 2107.93 (C₁₄₅H₁₂₀N₆O₆Zn). λ_{abs} = 423, 509, 541 nm; λ_{em} (λ_{ex} = 510 nm) 568, 600, 642 nm.

Zinc(II) 5-(3,5-Diethynylphenyl)-10,15,20-trimesitylporphyrin (6). Following a standard procedure for mixed-aldehyde condensations¹⁸ at high concentration²⁰ with BF₃·O(Et)₂–ethanol cocatalysis,¹⁹ samples of **5** (100 mg, 0.649

mmol), mesitaldehyde (289 mg, 1.95 mmol), and pyrrole (182 μL, 2.60 mmol) were condensed in CHCl₃ (36 mL) in the presence of BF₃·O(Et)₂ (80 μL, 0.633 mmol) at room temperature for 1.5 h. Then, DDQ (441 mg, 1.95 mmol) was added. After 1 h, TEA was added and the crude mixture was passed through a silica column [CHCl₃/hexanes (1:1)], affording a mixture of porphyrins. The resulting porphyrin mixture was treated with Zn(OAc)₂·2H₂O (712 mg, 3.25 mmol) in CHCl₃ (40 mL) and methanol (10 mL) overnight at room temperature. The organic phase was washed with water and dried over Na₂SO₄. Two column chromatography procedures [silica, CH₂Cl₂/hexanes (1:1) and (2:3)] afforded a purple solid (78.6 mg, 14%): ¹H NMR δ 1.84 (s, 12H), 1.85 (s, 6H), 2.64 (m, 9H), 3.16 (s, 2H), 7.28 (m, 6H), 8.02 (m, 1H), 8.32–8.33 (m, 2H), 8.70–8.73 (m, 4H), 8.77 (d, *J* = 5.1 Hz, 2H), 8.80 (d, *J* = 5.1 Hz, 2H); LDMS obsd, 852.49 [M⁺]. FABMS obsd, 850.3041; calcd, 850.3014 (C₅₇H₄₆N₄Zn). λ_{abs} = 423, 549 nm; λ_{em} (λ_{ex} = 550 nm) 593, 644 nm.

Zinc(II) 5-[3,5-Bis[2-[4-[9-(4-*tert*-butylphenoxy)perylene-3,4-dicarboximido]-3,5-diisopropylphenyl]ethynyl]phenyl]-10,15,20-trimesitylporphyrin (7). A mixture of **6** (40.0 mg, 46.9 μmol), **3** (73.0 mg, 103 μmol), Pd₂(dba)₃ (9.4 mg, 10 μmol), and P(*o*-tol)₃ (18.8 mg, 61.8 μmol) in toluene/triethylamine [5.0 mL (10:1)] was stirred at 60 °C under argon. After 3.5 h, another identical batch of catalyst was added. After 15.5 h, the mixture was cooled and passed through a silica column (CHCl₃). Preparative SEC (THF) and two column chromatography procedures [silica, CHCl₃/hexanes (9:1) and CHCl₃] followed by trituration with hexanes afforded a red solid (12.8 mg, 13%): ¹H NMR δ 1.18 (d, *J* = 6.6 Hz, 24H), 1.37 (s, 18H), 1.87 (m, 18H), 2.63–2.64 (m, 9H), 2.71–2.80 (m, 4H), 6.97 (d, *J* = 8.8 Hz, 2H), 7.12 (d, *J* = 8.8 Hz, 4H), 7.28 (m, 2H), 7.29 (m, 4H), 7.47 (d, *J* = 8.8 Hz, 4H), 7.53–7.58 (m, 4H), 7.67–7.72 (m, 2H), 8.24 (m, 1H), 8.30 (d, *J* = 8.1 Hz, 2H), 8.43 (d, *J* = 8.8 Hz, 2H), 8.42 (m, 2H), 8.456 (d, *J* = 8.1 Hz, 2H), 8.464 (d, *J* = 8.8 Hz, 2H), 8.55 (d, *J* = 7.3 Hz, 2H), 8.61 (d, *J* = 8.1 Hz, 2H), 8.65 (d, *J* = 8.1 Hz, 2H), 8.70–8.72 (m, 4H), 8.82 (d, *J* = 4.4 Hz, 2H), 8.95 (d, *J* = 5.1 Hz, 2H). MALDI-MS obsd, 2108.87 [M⁺]; calcd av mass, 2107.93 (C₁₄₅H₁₂₀N₆O₆Zn). λ_{abs} = 424, 511, 544 nm; λ_{em} (λ_{ex} = 510 nm) 593, 644 nm.

Zinc(II) 5,15-Bis(3,5-diethynylphenyl)-10,20-dimesitylporphyrin (9). Samples of **5** (80.0 mg, 0.519 mmol) and **8** (137 mg, 0.519 mmol) were condensed in CH₂Cl₂ (52 mL) in the presence of TFA (71.0 μL, 0.928 mmol) at room temperature for 30 min. Then, DDQ (118 mg, 0.519 mmol) was added. After 1 h, TEA was added and the crude mixture was passed through a silica column (CH₂Cl₂), affording a mixture of porphyrins. The resulting porphyrin mixture was treated with Zn(OAc)₂·2H₂O (570 mg, 2.60 mmol) in CHCl₃ (20 mL) and methanol (5.0 mL) overnight at room temperature. The organic phase was washed with water and dried over Na₂SO₄. Column chromatography [silica, CH₂Cl₂/hexanes (1:1)] afforded a purple solid (33.2 mg, 15%): ¹H NMR δ 1.82 (s, 12H), 2.64 (s, 6H), 3.16 (s, 4H), 7.29 (m, 4H), 8.03 (m, 2H), 8.33 (m, 4H), 8.80 (d, *J* = 4.4 Hz, 4H), 8.83 (d, *J* = 4.4 Hz, 4H); LDMS obsd, 858.86 [M⁺]. FABMS obsd, 856.2563; calcd, 856.2544 (C₅₈H₄₀N₄Zn). λ_{abs} = 424, 549 nm; λ_{em} (λ_{ex} = 550 nm) 596, 645 nm.

3,5-Bis[2-[4-[1,6,9-tris(4-*tert*-butylphenoxy)perylene-3,4-dicarboximido]-3,5-diisopropylphenyl]ethynyl]benzaldehyde, Method A (13). A mixture of **10** (281 mg, 280 μmol), **5** (22.0 mg, 140 μmol), Pd₂(dba)₃ (43.0 mg, 46.8 μmol), and P(*o*-tol)₃ (86.0 mg, 281 μmol) in toluene/triethylamine [28 mL (5:1)] was stirred at 60 °C under argon. After 3 h, another identical batch of catalyst was added. After 2 h, the mixture was cooled and passed through a silica column (CHCl₃). Preparative SEC (THF) and column chromatography (silica, CHCl₃) afforded a magenta solid (25.0 mg, 8.9%): mp > 230 °C; ¹H NMR δ 1.17 (d, *J* = 6.6 Hz, 24H), 1.32 (s, 18H), 1.34 (s, 18H), 1.35 (s, 18H), 2.68–2.75 (m, 4H), 6.90 (d, *J* = 8.8 Hz, 2H), 7.02 (d, *J* = 8.8 Hz, 4H), 7.08 (d, *J* = 8.8 Hz, 4H), 7.09 (d, *J* = 8.1 Hz, 4H), 7.37 (d, *J* = 8.8 Hz, 4H), 7.41 (d, *J* = 8.8 Hz, 4H), 7.42 (d, *J* = 8.8 Hz, 4H), 7.48 (m, 4H), 7.62–7.67 (m, 2H),

8.00 (m, 3H), 8.31 (s, 2H), 8.34 (s, 2H), 8.49 (d, $J = 8.8$ Hz, 2H), 9.25 (d, $J = 8.8$ Hz, 2H), 9.45 (d, $J = 8.1$ Hz, 2H), 10.03 (s, 1H); ^{13}C NMR δ 24.1, 29.3, 29.9, 31.7, 34.6, 87.3, 92.1, 111.8, 118.4, 118.5, 120.0, 120.4, 121.4, 122.3, 123.6, 123.8, 124.5, 124.9, 125.1, 125.2, 126.0, 126.7, 127.1, 127.3, 127.4, 127.86, 127.93, 128.2, 130.0, 130.2, 130.9, 131.8, 132.06, 132.13, 136.8, 139.9, 146.6, 147.2, 147.3, 147.8, 152.7, 153.5, 153.6, 156.3, 163.4, 191.1. MALDI-MS obsd, 2005.14; calcd av mass, 2002.51 ($\text{C}_{139}\text{H}_{128}\text{N}_2\text{O}_{11}$). $\lambda_{\text{abs}} = 415, 537$ nm; $\lambda_{\text{em}} (\lambda_{\text{ex}} = 540$ nm) 579, 624 (sh) nm.

3,5-Bis[2-[4-[1,6,9-tris(4-*tert*-butylphenoxy)perylene-3,4-dicarboximido]-3,5-diisopropylphenyl]ethynyl]benzaldehyde, Method B (13). A mixture of **11** (412 mg, 434 μmol), **12** (48.0 mg, 181 μmol), $\text{Pd}_2(\text{dba})_3$ (17.0 mg, 18.1 μmol), PPh_3 (29.0 mg, 109 μmol), and CuI (8.0 mg, 43 μmol) in toluene/triethylamine [36 mL (5:1)] was stirred at 50 °C under argon. After 3 h, another identical batch of catalyst was added. After 20 h, the mixture was cooled and passed through a silica column [$\text{CHCl}_3/\text{hexanes}$ (4:1)]. Preparative SEC (THF) and column chromatography [silica, $\text{CHCl}_3/\text{hexanes}$ (9:1)] afforded a magenta solid (240 mg, 66%): Analytical data were identical to those as described above.

Zinc(II) 5-[3,5-Bis[2-[4-[1,6,9-tris(4-*tert*-butylphenoxy)perylene-3,4-dicarboximido]-3,5-diisopropylphenyl]ethynyl]phenyl]-10,15,20-trimesitylporphyrin (14). Following a standard procedure for mixed-aldehyde condensations¹⁸ at high concentration²⁰ with $\text{BF}_3 \cdot \text{O}(\text{Et})_2$ -ethanol cocatalysis,¹⁹ samples of **13** (100 mg, 49.9 μmol), mesitaldehyde (22.2 mg, 150 μmol), and pyrrole (14 μL , 200 μmol) were condensed in CHCl_3 (2.8 mL) in the presence of $\text{BF}_3 \cdot \text{O}(\text{Et})_2$ (6.2 μL , 49 μmol) at room temperature for 1.5 h. Then, DDQ (34 mg, 150 μmol) was added. After 1 h, TEA was added and the crude mixture was passed through a silica column [$\text{CH}_2\text{Cl}_2/\text{hexanes}$ (2:1)], affording a porphyrin mixture. The resulting porphyrin was treated with $\text{Zn}(\text{OAc})_2 \cdot 2\text{H}_2\text{O}$ (55 mg, 250 μmol) in CH_2Cl_2 (10 mL) and methanol (3.0 mL) at room temperature for 12 h. The organic phase was washed with water and dried over Na_2SO_4 . Preparative SEC (THF) and column chromatography [silica, $\text{CH}_2\text{Cl}_2/\text{hexanes}$ (1:1)] afforded a red solid (24.3 mg, 18%): ^1H NMR δ 1.13 (d, $J = 6.6$ Hz, 24H), 1.31 (s, 18H), 1.33 (s, 18H), 1.34 (s, 18H), 1.85–1.86 (m, 18H), 2.63–2.71 (m, 13H), 6.89 (d, $J = 8.8$ Hz, 2H), 7.01 (d, $J = 8.8$ Hz, 4H), 7.06 (d, $J = 8.8$ Hz, 4H), 7.09 (d, $J = 8.8$ Hz, 4H), 7.28 (m, 6H), 7.35 (d, $J = 8.8$ Hz, 4H), 7.40 (d, $J = 8.1$ Hz, 4H), 7.43 (d, $J = 8.8$ Hz, 4H), 7.50 (m, 4H), 7.61–7.66 (m, 2H), 8.20 (m, 1H), 8.29 (s, 2H), 8.32 (s, 2H), 8.39 (m, 2H), 8.48 (d, $J = 8.1$ Hz, 2H), 8.71 (m, 4H), 8.79 (d, $J = 5.1$ Hz, 2H), 8.91 (d, $J = 4.4$ Hz, 2H), 9.24 (d, $J = 9.5$ Hz, 2H), 9.44 (d, $J = 8.1$ Hz, 2H). MALDI-MS obsd, 2694.31 [M^+]; calcd av mass, 2700.74 ($\text{C}_{185}\text{H}_{168}\text{N}_6\text{O}_{10}\text{Zn}$). $\lambda_{\text{abs}} = 424, 508, 543$ nm; $\lambda_{\text{em}} (\lambda_{\text{ex}} = 540$ nm) 593, 644 nm.

Zinc(II) 5,15-Bis[3,5-bis[2-[4-[1,6,9-tris(4-*tert*-butylphenoxy)perylene-3,4-dicarboximido]-3,5-diisopropylphenyl]ethynyl]phenyl]-10,20-dimesitylporphyrin (15). Samples of **13** (50.0 mg, 25.0 μmol) and **8** (6.6 mg, 25 μmol) were condensed in CH_2Cl_2 (2.5 mL) in the presence of TFA (3.5 μL , 45 μmol) at room temperature for 30 min. Then, DDQ (8.6 mg, 38 μmol) was added. After 1 h, TEA was added and the crude mixture was passed through a silica column [$\text{CH}_2\text{Cl}_2/\text{hexanes}$ (3:1)]. The resulting porphyrin was treated with $\text{Zn}(\text{OAc})_2 \cdot 2\text{H}_2\text{O}$ (14 mg, 63 μmol) in CH_2Cl_2 (8.0 mL) and methanol (2.0 mL) at room temperature for 12 h. The organic phase was washed with water and dried over Na_2SO_4 . Column chroma-

tography [silica, $\text{CHCl}_3/\text{hexanes}$ (3:1)] followed by trituration with methanol afforded a red solid (16.1 mg, 28%): ^1H NMR δ 1.12 (d, $J = 6.6$ Hz, 48H), 1.30 (s, 36H), 1.33 (s, 36H), 1.34 (s, 36H), 1.85 (s, 12H), 2.64–2.71 (m, 14H), 6.89 (d, $J = 8.8$ Hz, 4H), 7.00 (d, $J = 8.8$ Hz, 8H), 7.06 (d, $J = 6.6$ Hz, 8H), 7.09 (d, $J = 6.6$ Hz, 8H), 7.29 (m, 4H), 7.35 (d, $J = 8.8$ Hz, 8H), 7.39 (d, $J = 6.6$ Hz, 8H), 7.42 (d, $J = 6.6$ Hz, 8H), 7.49 (m, 8H), 7.61–7.66 (m, 4H), 8.20 (m, 2H), 8.28 (s, 4H), 8.32 (s, 4H), 8.40–8.41 (m, 4H), 8.47 (d, $J = 8.8$ Hz, 4H), 8.83 (d, $J = 4.4$ Hz, 4H), 8.95 (d, $J = 5.1$ Hz, 4H), 9.24 (d, $J = 8.8$ Hz, 4H), 9.44 (d, $J = 8.1$ Hz, 4H); MALDI-MS obsd, 4552.50 [M^+], 4402.44 [($\text{M} - 4-t\text{-Bu-Ph-O}$) $^+$]; calcd av mass, 4555.07 ($\text{C}_{314}\text{H}_{284}\text{N}_8\text{O}_{20}\text{Zn}$). $\lambda_{\text{abs}} = 426, 508, 538$ nm; $\lambda_{\text{em}} (\lambda_{\text{ex}} = 540$ nm) 596, 645 nm.

Zinc(II) meso-Tetrakis[3,5-bis[2-[4-[1,6,9-tris(4-*tert*-butylphenoxy)perylene-3,4-dicarboximido]-3,5-diisopropylphenyl]ethynyl]phenyl]porphyrin (16). Following a procedure for cocatalysis with $\text{BF}_3 \cdot \text{O}(\text{Et})_2$ + salt,³⁰ samples of **13** (48.0 mg, 24.0 μmol) and pyrrole (1.7 μL , 24 μmol) were condensed in CH_2Cl_2 (2.4 mL) in the presence of $\text{BF}_3 \cdot \text{O}(\text{Et})_2$ [3.0 μL of a 0.81 mM stock solution of $\text{BF}_3 \cdot \text{O}(\text{Et})_2$ in CH_2Cl_2 , 2.4 μmol] and NaCl (35 mg, 600 μmol) at room temperature for 1 h. Then, DDQ (4.1 mg, 18 μmol) was added. After 1 h, TEA was added and the crude mixture was passed through a silica column [$\text{CHCl}_3/\text{acetone}$ (49:1)] followed by preparative SEC (THF). The resulting porphyrin was treated with $\text{Zn}(\text{OAc})_2 \cdot 2\text{H}_2\text{O}$ (6.6 mg, 30.0 μmol) in CHCl_3 (5.0 mL) and methanol (1.0 mL) at room temperature for 12 h. The organic phase was washed with water and dried over Na_2SO_4 . Column chromatography [silica, $\text{CHCl}_3/\text{hexanes}$ (4:1)] followed by trituration with methanol afforded a red solid (15.4 mg, 31%): ^1H NMR δ 1.11 (d, $J = 6.6$ Hz, 96H), 1.27 (s, 72H), 1.29 (s, 72H), 1.36 (s, 72H), 2.62–2.71 (m, 16H), 6.87 (d, $J = 9.5$ Hz, 8H), 6.98 (d, $J = 8.8$ Hz, 16H), 7.04 (d, $J = 8.8$ Hz, 16H), 7.07 (d, $J = 8.1$ Hz, 16H), 7.32 (d, $J = 8.8$ Hz, 16H), 7.36 (d, $J = 8.8$ Hz, 16H), 7.41 (d, $J = 8.8$ Hz, 16H), 7.51 (m, 16H), 7.58–7.63 (m, 8H), 8.23 (m, 4H), 8.27 (s, 8H), 8.30 (s, 8H), 8.43–8.46 (m, 16H), 9.11 (m, 8H), 9.22 (d, $J = 8.8$ Hz, 8H), 9.41 (d, $J = 7.3$ Hz, 8H). MALDI-MS obsd, 8252.92 [M^+], 8104.44 [($\text{M} - (4-t\text{-Bu-Ph-O})$) $^+$], 7961.46 [($\text{M} - 2 \times (4-t\text{-Bu-Ph-O})$) $^+$], 7483.56 [($\text{M} - 5 \times (4-t\text{-Bu-Ph-O})$) $^+$], 7334.92 [($\text{M} - 6 \times (4-t\text{-Bu-Ph-O})$) $^+$]; calcd av mass, 8263.66 ($\text{C}_{572}\text{H}_{516}\text{N}_{12}\text{O}_{40}\text{Zn}$). $\lambda_{\text{abs}} = 431, 507, 533$ nm; $\lambda_{\text{em}} (\lambda_{\text{ex}} = 530$ nm) 564 (sh), 598, 648 nm.

Acknowledgment. This work was supported by the NSF (Grant CHE-9988142). Mass spectra were obtained at the Mass Spectrometry Laboratory for Biotechnology at North Carolina State University. Partial funding for the facility was obtained from the North Carolina Biotechnology Center and the National Science Foundation.

Supporting Information Available: ^1H NMR and LDMS (or MALDI-MS) of all new compounds; experimental procedures for the synthesis of the atropisomers of a 9-ethynyl-substituted bis(perylene)porphyrin; and energy-transfer simulations. This material is available free of charge via the Internet at <http://pubs.acs.org>.

JO0258002